Economic Geology, v. 103, pp. 1411–1435

Geochemistry and Evolution of Mississippi Valley-Type Mineralizing Brines from the Tri-State and Northern Arkansas Districts Determined by LA-ICP-MS Microanalysis of Fluid Inclusions

B. Stoffell,

Department of Earth Science and Engineering, Imperial College London, South Kensington Campus, Exhibition Road, London SW7 2AZ, United Kingdom

M. S. Appold,†

Department of Geological Sciences, University of Missouri, Columbia, 101 Geological Sciences Building, Columbia, Missouri 65211

J. J. Wilkinson,

Department of Earth Science and Engineering, Imperial College London, South Kensington Campus, Exhibition Road, London SW7 2AZ, United Kingdom, and Department of Mineralogy, Natural History Museum, Cromwell Road, London SW7 5BD, United Kingdom

N. A. McClean,

Department of Geoscience, University of Iowa, 121 Trowbridge Hall, Iowa City, Iowa 52242

and T. E. Jeffries

Department of Mineralogy, Natural History Museum, Cromwell Road, London SW7 5BD, United Kingdom

Abstract

The Tri-State and Northern Arkansas districts of the Ozark plateau, North America, are both classic examples of Mississippi Valley-type (MVT) mineralization, formed by continent-scale basinal brine migration as a result of the uplift of the Arkoma foreland basin in response to the Early Permian Ouachita orogeny. The chemistry of the fluids responsible for both sulfide mineralization and gangue precipitation in these districts was studied by quantitative microanalysis of individual fluid inclusions in quartz and sphalerite using 213-nm laser ablation-inductively coupled plasma-mass spectrometry (LA-ICP-MS).

Using halogen systematics, an evaporative seawater origin for the brines was determined, but higher Br concentrations suggest that the sphalerite-hosted "ore fluids" underwent a significantly greater degree of evaporation in the initial stages of fluid evolution compared to brines hosted by gangue phases. Metal contents of the brines responsible for quartz and dolomite precipitation are low compared to modern basinal brines, but many of the fluid inclusions trapped in sphalerite in both districts contained anomalously high metal concentrations, suggesting that mineralization involved incursion of a metal-rich fluid of distinct geochemistry. Examination of the multicomponent chemical characteristics revealed that dolomitization was probably an important process in the early chemical evolution of fluids that infiltrated both districts. In the Tri-State district, precipitation of sulfides was most likely driven by mixing of the metalliferous fluid with another brine, possibly rich in reduced sulfur. In northern Arkansas the compositional variations observed are best explained by local dissolution of the carbonate host rock. This may have been the process that ultimately drove sulfide deposition through fluid neutralization and reduction. Alternatively, the digestion of the host rock may have been the result of locally generated acidity produced by the deposition of sulfides.

The discovery of anomalously metal-rich fluids linked to mineralization suggests that these deposits are not simply the product of typical basin evolution, helping to explain the abundance of MVT mineralization in some forelands, whereas others are barren. It is likely that a significant portion of the history of the hydrothermal flow system was characterized by the precipitation of barren gangue assemblages from metal-poor brines, with metalliferous fluids only being expelled from a specific stratigraphic package at a distinct stage of basin evolution.

Introduction

Mississippi Valley-type (MVT) deposits have long been recognized to be products of the migration of sedimentary basinal brines generated from diagenetic processes in sedimentary basins (Garven et al., 1993; Garven, 1995; Leach et al., 2005). Although such fluids appear to be widespread in basins worldwide, ore-grade MVT occurrences are comparatively rare, implying that special conditions must be invoked to explain their formation. One possible factor is that the mineralizing brines were relatively enriched in base metals compared to typical basinal brines. Determining the metal content of the fluids responsible for forming MVT deposits is accepted as a key requirement in understanding their origin and their relationship to sedimentary diagenesis (Anderson, 1975), but few attempts have been made to measure the base metal contents of paleo-ore fluids preserved in fluid inclusions from

† Corresponding author: e-mail, appoldm@missouri.edu

MVT deposits, and how MVT ore fluids compare with contemporary sedimentary brines with respect to metal concentrations is not well documented.

Chemical analyses indicate that modern basinal brines rarely have metal concentrations exceeding 100 ppm Pb, 250 ppm Zn, about 3 ppm Cu, and about 150 ppm Ba (Carpenter et al., 1974; Collins, 1975; Kharaka et al., 1987; Land et al., 1988; Stueber and Walter, 1991; Land, 1995; Hanor, 1996). Concentrations can vary over two orders of magnitude below these approximate maximum values. Theoretical solubility relationships can also be used to assess possible metal contents of ore fluids (Anderson, 1975; Barnes, 1979; Barrett and Anderson, 1988; Hanor, 1996; Seward and Barnes, 1997). However, the calculated metal concentrations strongly depend on the pH, dissolved sulfur content, and redox potential of the fluid, none of which are particularly well constrained for MVT systems. These uncertainties allow for variations in metal content of the ore fluid of several orders of magnitude, extending well beyond the maximum concentrations observed in contemporary sedimentary brines. Therefore, in most MVT districts, the metal content of the mineralizing brine must be regarded as essentially unknown.

The earliest reported analyses of metals in MVT fluid inclusions are from fluorite from the Illinois-Kentucky fluorite district and used neutron activation (Czamanske et al., 1963) and atomic absorption (Pinckney and Hafty, 1970). Measured Cu and Zn concentrations were reported to be as high as 10,900 and 9,100 ppm, respectively. McLimans (1977) used atomic absorption to analyze fluid inclusions in barite and calcite from the Upper Mississippi Valley district in southwest Wisconsin, finding concentrations of up to 500 ppm Pb, 8,100 ppm Zn, and 5,100 ppm Cu. However, these studies all used bulk sampling methods, so that the high metal values may actually reflect contamination from metal sulfide mineral inclusions rather than true fluid compositions.

Advances in LA-ICP-MS technology in the last two decades (e.g., Jeffries et al., 1998) have provided the means for analyzing single fluid inclusions (Günther et al., 1997, 1998; Stoffell et al., 2004) and thus a greatly improved method for characterizing ore fluid metal content. The first application of LA-ICP-MS to fluid inclusions in MVT deposits was by Shepherd and Chenery (1995), who used a 266-nm UV laser to analyze fluid inclusions in fluorite from the North Pennines and southwest England. They reported concentrations of up to 25,000 ppm Pb, 7,100 ppm Zn, and 1,100 ppm Cu. A later study of brine fluid inclusions in quartz from base metal mineralized veins in southwest England using the shorter wavelength 213-nm UV laser yielded much lower concentrations of up to 295 ppm Pb and 86 ppm Zn (Stoffell et al., 2004). Appold et al. (2004) used 266-nm LA-ICP-MS to study fluid inclusions in gangue minerals from the Southeast Missouri district. They found that the Pb, Zn, and Cu concentrations of the fluids responsible for depositing gangue, which does not directly overlap the paragenetic stages of sulfide mineral deposition in this district (Hagni, 1986), were below instrumental detection limits, typically around 10 ppm but up to 10^3 ppm in small inclusions.

The aim of this study was the chemical characterization of fluid inclusions trapped in ore and gangue phases in the Tri-State and Northern Arkansas MVT districts of the Ozark plateau, United States. These data have been used to test hypotheses for the origins of the mineralizing fluids and theoretical models of ore metal transport and deposition. The Tri-State and Northern Arkansas regions were selected for study because they are classic and representative examples of the MVT deposit class and also contain a significant amount of transparent quartz and pale sphalerite in the ore assemblage that are amenable to fluid inclusion studies. Furthermore, both regions have a long history of research and occur in a terrane that has been well characterized geologically and hydrologically, providing a firm research framework within which the results can be interpreted. It is hoped that this study will help better to define where MVT deposits sit within the broader context of foreland basin diagenesis and to address, among other things, whether MVT districts formed from fluids that were anomalously enriched in metals or represent environments that were particularly efficient at extracting metals from fluids that had typical basinal brine compositions.

Geologic Background

The Ozark plateau of the North American midcontinent represents one of the richest provinces of sediment-hosted base metal sulfide mineralization in the world. This mineralization occurs principally in MVT deposits concentrated in at least four districts in southeast Missouri, central Missouri, northern Arkansas, and the Tri-State region of Oklahoma, Missouri, and Kansas (Fig. 1). At over 900 million (M) and 500 M short tons of ore, respectively, the Southeast Missouri and the Tri-State districts represent the world's two largest occurrences of MVT mineralization (Brockie et al., 1968; Ohle and Gerdermann, 1989). Smaller accumulations of MVT mineralization occur in the Northern Arkansas and Central Missouri districts. Production records are incomplete, but the Northern Arkansas district yielded at least 24,000 short tons of zinc and 1,500 short tons of lead metal (McKnight, 1935), and the Central Missouri district yielded at least 350,000 short tons of barite, 17,000 short tons of galena, and 6,000 short tons of sphalerite (Leach, 1994).

The Ozark MVT deposits are believed to be an expression of regional sedimentary diagenesis and tectonism, formed from invading sedimentary brines during uplift of the Arkoma foreland basin. This was driven by the Ouachita orogeny in the Late Pennsylvanian to Early Permian (Wu and Beales, 1981; Wisniowieki et al., 1983; Leach and Rowan, 1986; Pan et al., 1990; Viets and Leach, 1990; Garven et al., 1993; Leach, 1994; Appold and Garven, 1999; Nunn and Lin, 2002; Appold and Nunn, 2005). Uplift of the Ozark plateau occurred as a flexural response to crustal thickening in the Ouachitas and led to doming and a rectilinear pattern of northwest-southeast– and southwest-northeast–trending normal faults. Flexural downwarping occurred in the Arkoma basin, providing the accommodation space for thick sequences of Pennsylvanian-Permian-age flysch and molasse, most of which have since been removed by erosion. This thick sequence likely served as a thermally insulating regional cap and aquitard and may have helped produce the anomalously warm temperatures recorded across the foreland during this time (Appold and Nunn, 2005).

As the Ouachita orogeny waned, and erosion began to dominate over uplift, the foreland began to rebound with the

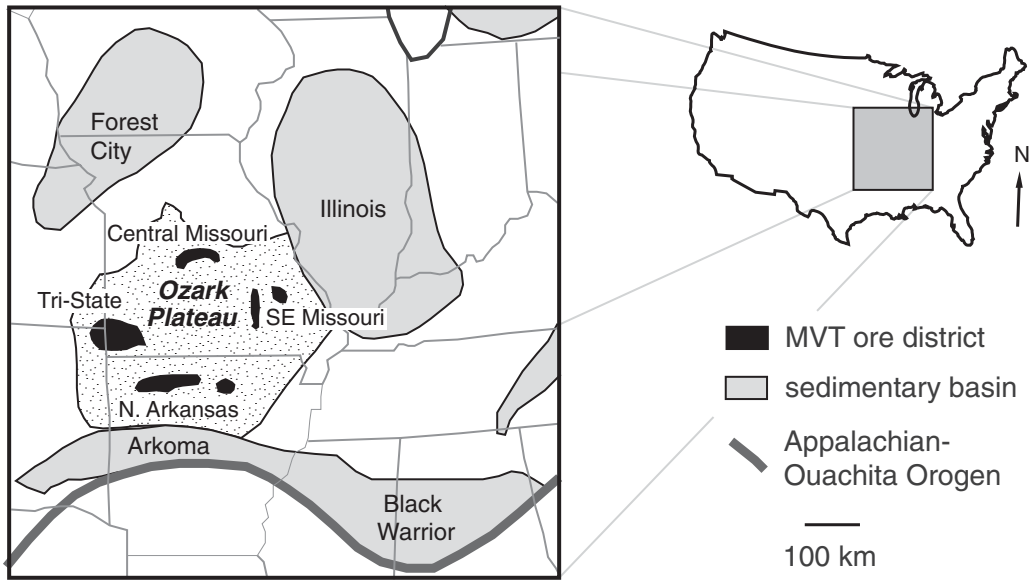

FIG. 1. Mississippi Valley-type (MVT) deposits of the Ozark plateau.

decrease in mass of the fold-thrust belt-producing topographic gradients that set in motion the ground-water flow regime that is believed to have formed the Ozark MVT deposits (Garven et al., 1993).

Ozark mineralization

In the Tri-State district, mineralization occurs principally in six Zn-Pb orebodies hosted by cherty Mississippian limestones of the Boone Formation. The Boone Formation consists of numerous units of alternating chert and limestone, which in places is crinoidal or oolitic, and in the Baxter Springs member in particular is locally shaley and contains significant glauconite.

Ore mineralogy is dominated by sphalerite and galena, accompanied by minor amounts of chalcopyrite, pyrite, and marcasite. The main gangue minerals are dolomite and calcite with abundant silicification in the form of quartz, chert, and jasperoid (McKnight and Fischer, 1970). The Boone Formation has been subject to modest folding, fracturing, and karst-related brecciation and is part of a larger hydrostratigraphic package called the Springfield plateau aquifer. Beneath this aquifer is the low-permeability Ozark confining unit, which is known to thin significantly within the Tri-State district, and in places is absent altogether (Imes and Smith, 1990). These windows in the confining unit may have been critical in permitting the ascent of deep, heated brines into the host formations (Brockie et al., 1968).

In many places, ore is localized by folds that typically developed in response to displacements on deep-seated faults. A number of these faults extend to the Precambrian basement and may have served as important conduits for mineralizing fluids (Brockie et al., 1968; McKnight and Fischer, 1970; Hagni, 1976). This is based on the fact that they commonly intersect orebodies and are mineralized over intervals transecting multiple stratigraphic units.

Most Tri-State deposits are characterized by a distinctive lateral zonation (McKnight and Fischer, 1970), consisting of a central dolomite core surrounded successively by the main sulfide mineralization, a jasperoid zone, and finally unaltered and unmineralized limestone. Fluids entering the host formations at structural access points appear to have moved significant distances laterally, depositing ore in highly transmissive zones, particularly in areally extensive, karst-related breccias.

The mineral paragenesis is consistent throughout the district (Fig. 2). MVT mineralization began with the precipitation of a coarsely crystalline gray dolomite, an important exploration guide (Hagni, 1976). This was followed by jasperoid (locally coarsening into quartz), pink sparry dolomite, the main-stage sulfides, and calcite. Although gray dolomite deposition ended before the beginning of main-stage sulfide deposition, fine-grained sulfides are disseminated throughout the gray dolomite and impart to the mineral its color. The gray dolomite commonly grades into pink dolomite, which overlaps with sphalerite, galena, and chalcopyrite. The period of jasperoid deposition also overlaps that of the sulfides, which are commonly disseminated in the jasperoid (Brockie et al., 1968; McKnight and Fischer, 1970).

Zinc-lead deposits occur over a broad area in northern Arkansas, hosted primarily by carbonates of the Ordovician Everton and the Mississippian St. Joe and Boone Formations. These comprise alternating chert and limestone successions which are in places glauconitic and contain local shaley zones. Individual deposits are small, ranging up to 200 m in length, around 80 m in width, and 7 m in thickness (Long et al., 1986). The greatest amount of mineralization, about 41 percent of the total (Long et al., 1986), is in the Rush subdistrict, located in the west-central part of the area. As in the Tri-State district, mineralization is concentrated in strata-bound breccia bodies. However, in contrast to Tri-State, these breccias appear to have been largely controlled by structures rather than primarily by karstification, as they are typically associated with faults and gentle folds that fractured the host rock. Subsequent dissolution is also evident (McKnight, 1935;

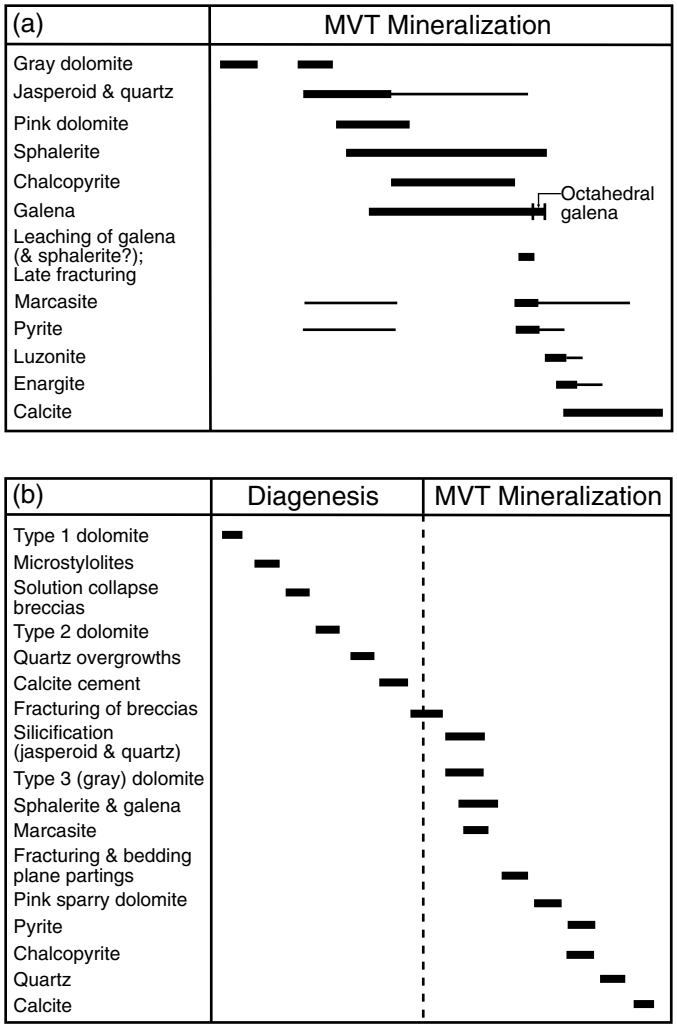

FIG. 2. Paragenetic sequence of diagenesis and MVT mineralization in the (a) Tri-State and (b) Northern Arkansas districts (modified after McKnight, 1935; Hagni and Grawe, 1964; Long et al., 1986).

Long et al., 1986). Many of the faults in the Northern Arkansas district contain MVT mineralization, although typically only in the upper reaches that transect the Boone Formation. Thus, as in the Tri-State district, faults appear to have been important conduits for mineralizing fluids.

The mineralogy and paragenesis of the deposits in northern Arkansas resemble those of the Tri-State district (Fig. 2). Sphalerite is the dominant sulfide mineral, followed by galena, chalcopyrite, pyrite, and marcasite. The principal gangue phases are dolomite, calcite, jasperoid, and quartz. The jasperoid and a fine, drusy quartz constitute an early and pervasive silicification event, accompanied closely in time by gray sparry dolomite. Sphalerite, galena, and marcasite deposition began after, but largely overlapped, the silica and gray sparry dolomite. These phases are followed by pink, sparry dolomite, which closely resembles that observed in the Tri-State district but is later in the paragenesis. Pyrite and chalcopyrite were precipitated next, followed by a second, much more coarsely crystalline variety of quartz, and finally calcite.

Genetic models for the Northern Arkansas and Tri-State districts have been presented by several authors. McKnight (1935) and McKnight and Fischer (1970) postulated a magmatic hydrothermal origin for the northern Arkansas mineralization, based primarily on mineralogical analogies to known magmatic hydrothermal ore deposits. White (1958) and Hagni (1976) advocated a sedimentary basinal brine origin for the Tri-State mineralization, based on fluid inclusion and sulfur isotope compositions. Deloule et al. (1986) extended the basinal brine genetic concept and argued that, based on the covariance of sulfur and lead isotope compositions in individual galena crystals from Tri-State, lead and sulfide must have been transported together in the mineralizing fluids. Plumlee et al. (1994) used geochemical reaction path modeling to evaluate a variety of possible precipitation mechanisms for the northern Arkansas and Tri-State mineralization. They found that for a saline, moderately acidic hydrothermal fluid saturated with respect to quartz, dolomite, sphalerite, and galena, the mineral parageneses and relative abundances could best be described by cooling and reaction with limestone, but stated that mixing with local sulfide-rich fluids may also have played a significant role.

Methodology

Sampling strategy

Samples of both mineralized and gangue material were collected from locations throughout the Tri-State and Northern Arkansas districts (Table 1). Unfortunately, because mining activity in Tri-State had largely ceased by the early 1970s, and because most of the mines have since flooded with water rendering them inaccessible, all of the Tri-State samples used in the study were collected from coarse spoil heaps and small mine dumps. However, these mine dumps are highly localized to the excavations from which they were derived, allowing sample location to be constrained to within a few tens of meters. Additionally, because the paragenesis of mineralization in the district is well known, the paragenetic stage represented by the samples can be confidently inferred. The Tri-State samples were taken from sites in the Oronogo-Duenweg, Joplin, Neck City, Granby, and Picher subdistricts, spanning a north-south distance of some 30 km. Samples containing coarse quartz were favored for analytical reasons; samples of pink dolomite gangue and ore-stage sphalerite were also collected.

All samples from northern Arkansas were collected in situ from the Monte Cristo and Philadelphia mines of the Rush subdistrict, within 0.5 km of each other, and the Lucky Dog mine of the Tomahawk Creek subdistrict, approximately 20 km to the southwest (Long et al., 1986). Samples of coarse quartz apparently intergrown with ore-stage sphalerite were only obtained from the Monte Cristo mine.

Microthermometry

Samples were prepared as standard doubly polished wafers approximately 150 μm thick and were mapped and studied in transmitted light prior to microthermometric analysis. Fluid inclusion microthermometry was performed using a Linkam™ THMSG600 heating-freezing stage, employing standard laboratory procedures (Shepherd et al., 1985). Stage calibration

TABLE 1. Locations of Samples Analyzed in This Study (latitude-longitude coordinates are reported relative to the WGS 84 datum)

Sample code	Latitude (°N)	Longitude (°W)	Location description
Northern Arkansas			
NALD 1	36.06567	92.74422	Lucky Dog mine, Tomahawk Creek subdistrict
NAMC 1	36.13052	92.55152	Monte Cristo mine, Rush Creek subdistrict
NAPA 1	36.13290	92.54938	Philadelphia mine, Rush Creek subdistrict
Tri-State			
TSBS 1	36.98504	94.74702	East Picher field near Baxter Springs, KS
TSBS 3	37.03271	94.75474	Northeast Picher field near Baxter Springs, KS
TSBS 4	37.00505	94.77327	Northeast Picher field near Baxter Springs, KS
TSCV 1	37.14615	94.43885	Oronogo-Duenweg trend near Carterville, MO
TSJ 1			Unspecified location; Univ. of Iowa collection
TSOR 2	37.17409	94.47243	Oronogo-Duenweg trend near Oronogo, MO
TSPC 1	36.96723	94.81153	South Picher field near Picher, OK
TSPC 2	36.96418	94.81046	South Picher field near Picher, OK
TSWB 2	37.01014	94.87187	Northwest Picher field near Treece, KS
TSWB 3	37.01468	94.86025	Northwest Picher field near Treece, KS
TSWC 1	37.15292	94.45368	Oronogo-Duenweg trend near Webb City, MO

was carried out at –56.6°, 0.0°, +10.0°, +30.4°, and 294°C using inhouse synthetic H_2O-CO_2 fluid inclusion standards. Measurement precision was ±0.1°C and estimated accuracy was ±0.2°C in the range of –60° to +200°C. The temperatures of ice melting and liquid-vapor homogenization were measured in all inclusions, and measurements of phase transitions were duplicated to ensure reliable data were obtained.

LA-ICP-MS microanalysis of individual fluid inclusions

Laser ablation analyses were carried out using a New-Wave UP213AI, 213-nm aperture-imaged laser ablation system (Jeffries et al., 1998) equipped with beam homogenization optics. Ablated particulate material was analyzed by a Thermo Element PlasmaQuad 3 ICP-MS with enhanced sensitivity S-option interface, housed in the Natural History Museum, London. The carrier gas used was a mixture of He and Ar, which improves the transport of the aerosol and reduces fractionation (Günther and Heinrich, 1999).

Prior to LA-ICP-MS analysis, samples and standards were fixed to a glass slide by low-contaminant tape and loaded into the sample chamber. The chamber was then purged with gas to avoid atmospheric contamination. In each experimental run, up to 20 separate analyses could be performed on standards and/or samples limited by the volume of data that can be handled by the processing software.

The experimental approach and calibration strategy are described in greater detail by Stoffell et al. (2004). Calibration (external standardization) was carried out at the beginning and end of each experimental run by ablating two pure silica glass capillaries with an external diameter of 350 μm, an internal diameter of 250 μm, and a length of 10 mm completely filled with a standard multielement solution and tipped with wax to prevent fluid loss. The laser beam diameter used was 13 μm, the same as that used for the inclusion analyses. This approach was adopted because it provides a good procedural and matrix-matched analog for the inclusion ablation process. Duplicate analyses of NIST 612 glass were also made at the start and end of each run as a control. For inclusion analyses, ablation commenced with an energy density below the ablation threshold for that particular mineral and was increased in small increments over approximately 10s until maximum energy density was reached, after which laser power was kept constant. This approach normally produces a clean, smooth-sided ablation pit with a regular, near-circular surface expression. For liquid-vapor inclusions without daughter minerals, ablation of large inclusions using a beam diameter smaller than the inclusion does not normally result in significant fractionation for any of the elements reported (Buckroyd, 2008), the exception being when catastrophic spalling of the inclusion occurs during opening (e.g., Stoffell et al., 2004).

Following laser ablation analyses, absolute quantification of fluid inclusion concentrations was achieved by first integrating the signal interval and subtracting the background contribution. Sensitivity for each element was then computed using the external standard, enabling calculation of element intensity ratios. Because the total volume of fluid released from an inclusion during laser ablation is unknown, an internal standard is required to convert these intensity ratios to absolute concentrations. This must be an element in the fluid, the concentration of which can be independently estimated. In this study the chloride concentration was used, estimated from ice-melting temperatures interpreted in the NaCl-H_2O system, and assuming that weight percent NaCl equivalent is a good approximation (within 5–10%) of the total salinity (Crawford, 1981). Extensive testing in the laboratory using synthetic fluid inclusions has shown that there is no significant difference in accuracy when using Cl as an internal standard versus other elements such as Na (Buckroyd, 2008). Cl has the advantage that its estimation via microthermometry, assuming chloride-rich brines are involved, is subject to less uncertainty than for cations (such as Na). As shown in Figure 3, the lower background for Cl compared to Na on the system used, and its high concentration in the highly saline inclusion fluids studied, led to the acquisition of strong signals well above background that justified its use as an internal standard (Günther et al., 1998). Data processing was carried out using the LAMTRACE package (S. Jackson, Macquarie University).

Quartz was the favored mineral host for the current study because it is relatively robust so that postentrapment modification of fluid inclusions is less likely than for softer minerals

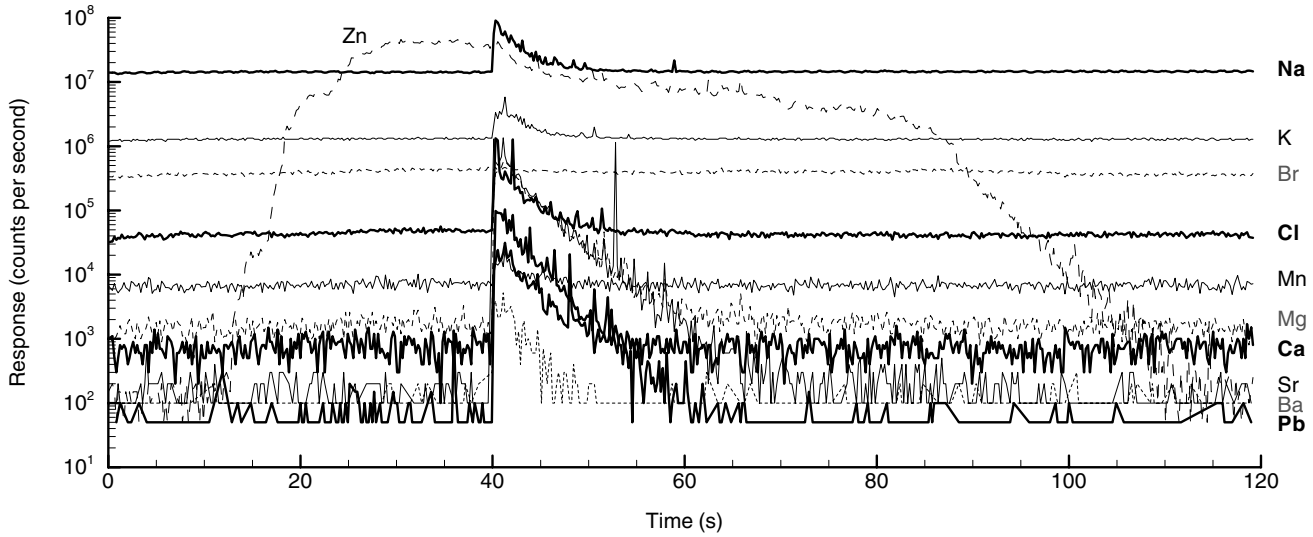

FIG. 3. Transient signal responses for LA-ICP-MS analysis of a sphalerite-hosted fluid inclusion, sample NAMC 1-2 A inclusion 1, from northern Arkansas (45 × 23 μm). The laser was turned on after about 10 s as indicated by the rapid rise in the Zn signal. The inclusion was breached at 40 s as indicated by the spike in elements present in the fluid such as Na, K, Ca, and Cl. All other elements detected display an identical release profile indicative of their presence in the aqueous phase as well. Note the large signal for Pb, quantified as 400 ppm.

such as carbonates, and quartz typically contains very low concentrations of any elements other than Si and O. However, the mineralogical complexity of natural systems dictates that a complete study of an ore-forming system must necessarily include analyses of fluids trapped in minerals other than quartz. Assuming these inclusions are primary and have not been subjected to any postentrapment modification (such as leakage or necking), then the fundamental obstacle to successful analyses in these matrices is the contamination of the inclusion signal by a contribution from the host.

An important breakthrough in this study was the successful analysis of fluid inclusions hosted within both the pink dolomite gangue (the most volumetrically significant gangue phase in the Tri-State district) and also the ore-stage sphalerite. This is particularly significant as it offers the opportunity to address the key question of whether the ore-forming fluid (which precipitated and subsequently became trapped within the sphalerite) displays any significant geochemical differences compared to the fluid responsible for precipitating the gangue assemblage.

The experimental procedure for dolomite and sphalerite was identical to that used for quartz-hosted inclusions and signals were processed using the same method. Subtraction of a mineral ablation background allowed estimation of elements in the fluid inclusions that were also present at low concentrations in the host mineral. Because the mass of the host mineral ablated during the actual fluid inclusion analysis is less than that in the mineral background interval, values returned for elements that are present in the host represent minimum concentrations for the fluid. However, due to the greater uncertainty in the background subtraction, a lower degree of confidence can be attached to results for elements that are present in the host mineral as detected during ablation prior to inclusion opening. For elements that are not detected in dolomite or sphalerite during ablation prior to inclusion breaching (e.g., Pb, Ba, Sr, Ca, Mg, Mn, Br, K, Na for the sphalerite-hosted inclusion shown in Fig. 3), the results should be just as reliable as inclusion analyses in quartz.

Confidence that the metal determinations, in particular for Pb in inclusions in sphalerite, are actually derived from aqueous signals rather than the host mineral is afforded by time-resolved plots of signal intensities (e.g., Fig. 3). In this, and other similar analyses, the zinc response increases early in the analysis when the laser is turned on and the sphalerite host is ablated. At about 40 sec, the fluid inclusion is ruptured as indicated by a sharp spike in the signals of Na, K, Ca, and Cl. These spikes are perfectly paralleled by the spike in the Pb (and Ba, Mg, Mn, Sr), indicating that the Pb signal is highly likely to be derived from the fluid inclusion. Although it is possible that a Pb-rich zone within the sphalerite matrix was encountered at the precise location where the fluid inclusion was ruptured, our experience from ablating small solid mineral inclusions shows that this would typically generate a signal with a broader, rounded form in contrast to the characteristic fluid release spike as seen in Figure 3. Because spikes in the Pb signals in the present study were consistently strongly correlated with spikes in known aqueous components like Na, Cl, K, and Ca, it is concluded that the high Pb concentrations represent aqueous rather than matrix responses.

Results

Sample and fluid inclusion petrology

Samples were studied in transmitted light to determine the relationships between different phases and also to identify and map accurately the location of large, primary fluid inclusions that should represent the fluid present at the time of hydrothermal mineral growth. Relatively large inclusions were selected preferentially because these have been shown to

yield more reproducible analyses and lower detection limits (Heinrich et al., 2003; Allan et al., 2005).

Individual sample locations are presented in Table 1. In the Tri-State district, quartz samples are typically coarse, with single crystals ranging from 1 to 10 mm in size. Sphalerite crystals are a few millimeters to 3 cm in size and range in color from pale brown to dark brown or red. The pink dolomite is very pale and coarsely crystalline, with individual crystals ranging from 3 to 6 mm in size. It typically displays open-space filling textures and is most commonly found in sharp contact with the earlier gray dolomite.

Although samples containing more than one of the three main mineral phases (quartz, sphalerite, and dolomite) were collected from some Tri-State locations, insufficient evidence was available to make a definitive judgment regarding the relative timing of each phase, partly because the samples were not in situ. In the rare samples containing both quartz and sphalerite, the sphalerite appears to have been the later phase, overgrowing the quartz. The paragenesis of the district has been well studied and both the quartz and pink dolomite are believed to have begun to precipitate early in the paragenetic sequence, prior to the onset of Zn-Pb-Cu sulfide mineralization, although both phases show a considerable overlap with the start of the main stage of sphalerite deposition (Fig. 2a; Brockie et al., 1968; McKnight and Fischer, 1970; Hagni, 1976).

All inclusions studied were two-phase (liquid + vapor) aqueous inclusions and were categorized as primary or secondary according to the criteria of Roedder (1984). Inclusion sizes ranged from <10 up to 124 μm in a single observed dimension and had mean dimensions of 47 × 23 and 45 × 24 μm in quartz and sphalerite, respectively. In quartz, the majority of inclusions classified as primary typically occurred in small, three-dimensional groups, with a small number found as larger, isolated inclusions. No quartz samples from the Tri-State district showed any evidence of growth zoning under transmitted light. Primary inclusions in sphalerite showed a very similar distribution, with most primary inclusions occurring in small three-dimensional groups of three to five inclusions or as isolated, typically larger inclusions. Some sphalerite crystals contained abundant secondary inclusions on fracture planes. These were typically small (<10 μm) and/or planar and were not analyzed as part of this study. No daughter minerals were observed in any inclusions in the samples from the Tri-State district. Fluid inclusions in pink dolomite were far less abundant and of a smaller size, with those analyzed averaging 24 × 15 μm in the two observed dimensions. These tended to be regular, relatively equant, square to rectangular in geometry and isolated within the sample rather than in groups.

In samples from the Northern Arkansas district, quartz typically is coarser grained than that found in the Tri-State district (0.5–2.5 cm), and in the Monte Cristo and Lucky Dog mines of the Rush Creek subdistrict these are associated with equally coarse, pale yellow sphalerite. In these samples the quartz appears to overgrow and therefore probably postdates pale sphalerite, in agreement with the observations of previous workers (Potter, 1971; Long et al., 1986), who considered the coarse quartz to be late in the paragenesis, after both main-stage sphalerite and the subsequent pink dolomite.

In the northern Arkansas samples, all inclusions studied were two-phase (liquid + vapor) aqueous type. Most quartz crystals were not strongly growth zoned, and primary inclusions were found to occur either as single, typically large and relatively equant inclusions or small three-dimensional groups of inclusions not spatially related to fractures and distributed randomly throughout the crystal. In crystals that did display growth zoning, inclusions within the zones tended to be highly irregular, three-dimensional, and elongated in the direction of crystal growth, giving a high level of confidence that these inclusions are primary.

A small number of the quartz-hosted inclusions observed occurred in microfractures and were ignored because they are unlikely to represent the fluid present during mineral growth. Some inclusions showed evidence of necking down; however, the homogenization temperatures of these inclusions are generally similar to those around them suggesting that necking down occurred at relatively elevated temperatures, prior to nucleation of the bubble. No daughter crystals were observed in any of the inclusions studied. Inclusions ranged from 140 to <10 μm in the two observed dimensions with a mean of 50 × 22 μm. Inclusions analyzed in sphalerite were of similar average dimensions (50 × 24 μm) and had a similar distribution to those in quartz, with most primary inclusions occurring in small, three-dimensional groups or isolated.

Microthermometry

The microthermometric data gathered from all inclusions analyzed are given in Table 2 and are summarized in Table 3. These data define a number of fluid types (Fig. 4, Table 4). In samples from the Tri-State district, the fluid salinities and homogenization temperatures (T_h) as a whole are variable, although the bulk of the data are within the range of 21 to 25 wt percent NaCl equiv and 80º to 130ºC, respectively. The dolomite-hosted inclusions (with the exception of one significantly less saline outlier considered to be secondary) are relatively saline (21–24 wt % NaCl equiv: Fig. 4), show a range of T_h from ~80º to 130ºC, and overlap with inclusion data from both quartz and sphalerite. A second group of data (derived from sphalerite samples TSBS 4-5, 4-6, and 1-7) spread to lower T_h values and lower salinities (as low as ~17.5 wt %), with inclusions hosted by quartz sample TSPC lying at the end of this array at salinities of around 16 wt percent and homogenization temperatures of around 60ºC. Hereafter, the higher salinity group is referred to as "type 1_{TS}" Tri-State fluid, and the lower salinity inclusions of sample TSPC-1 are referred to as "type 2_{TS}," with the intermediate-salinity fluid preserved in the TSBS sphalerite samples referred to as "transitional." Summary descriptions of each of these fluid types are given in Table 4. The two inclusions analyzed in quartz sample TSCV-1-2 show significantly higher homogenization temperatures than the rest of the data, but there is no evidence that these are unreliable. A very high homogenization temperature in an isolated inclusion in sample TSOR-2 is considered to be a product of necking down. As a whole, the trends in the data could be explained by a combination of cooling and mixing of the type 1_{TS} and 2_{TS} fluids, with the different samples trapping inclusions at different stages of this evolution. Quartz, which has a broad paragenetic distribution,

TABLE 2. Microthermometry and LA-ICP-MS Analyses of Fluid Inclusions from the Northern Arkansas and Tri-State Districts (all elemental concentrations are shown in parts per million)

Sample ID	Inclusion no.	Size[1] (μm)	T_h (°C)	Salinity[2]	Li	Na	Mg	Cl	K	Ca	Mn	Cu	Zn	Br	Sr	Ba	Pb
Northern Arkansas quartz																	
Very coarse, open-space filling quartz intergrown with sphalerite																	
NAMC 1 B	1	108 × 23	122.9	23.1	2.5E+01	8.2E+04	1.2E+00	1.4E+05	2.9E+03	1.5E+04	1.3E+00	<5.6E-01	<2.6E-01	8.1E+02	3.6E+02	1.2E+01	<7.5E-01
NAMC 1 B	2	34 × 25	122.9	23.1	7.5E+00	8.5E+04	6.3E+00	1.4E+05	4.6E+03	8.3E+03	<2.6E+00	<1.3E+00	<5.9E-01	<9.8E+02	1.4E+02	6.8E+00	2.5E-01
Mean[3]					1.6E+01		3.7E+00		3.7E+03	1.2E+04					2.5E+02	9.6E+00	
RSD[3] (%)					76.3		97.2		33.0	40.4					60.9	41.1	
NAMC 1 C6	1	44 × 12	115.4	22.4	2.6E+01	6.6E+04	5.6E+00	1.4E+05	9.2E+03	2.9E+04	1.8E+00	<1.5E+00	<6.9E-01	<2.1E+03	8.3E+02	1.8E+01	<1.2E+00
NAMC 1 C6	2	28 × 24	115.6	22.3	1.3E+01	7.9E+04	7.4E+00	1.4E+05	3.1E+03	1.5E+04	<4.3E-01	<5.3E-01	<2.5E-01	<1.3E+03	6.4E+02	7.4E+00	8.7E-01
NAMC 1 C6	3	33 × 27	115.0	23.6	2.0E+01	8.6E+04	9.1E+02	1.4E+05	3.0E+03	1.1E+04	7.5E-01	<2.3E-01	1.2E+00	2.5E+02	4.1E+02	5.9E+00	5.3E-01
NAMC 1 C6	5	65 × 15	120.0	23.4	1.6E+01	8.7E+04	2.8E+00	1.4E+05	2.1E+03	8.4E+03	1.5E-01	<1.7E-01	2.0E-01	1.6E+02	3.7E+02	5.8E+00	3.4E-01
NAMC 1 C6	6	69 × 27	113.8	22.8	1.6E+01	8.2E+04	1.5E+02	1.4E+05	3.2E+03	1.3E+04	8.3E-01	<2.4E-01	6.3E-01	3.0E+02	4.1E+02	6.4E+00	3.6E-01
NAMC 1 C6	7	26 × 23	110.8	22.6	6.1E+01	6.8E+04	2.4E+02	1.4E+05	9.9E+03	2.7E+04	<2.6E+00	<3.0E+00	<1.3E+00	<4.2E+02	4.1E+02	2.0E+01	3.5E+00
NAMC 1 C6	8	34 × 32	114.0	22.5	3.5E+01	7.7E+04	<1.4E+00	1.4E+05	1.9E+03	1.9E+04	<1.1E+00	<1.3E+00	5.0E+00	<1.6E+02	4.5E+02	2.5E+00	<8.6E-02
Mean[3]					2.7E+01		2.2E+02		4.6E+03	1.7E+04	8.7E-01		1.8E+00	2.4E+02	5.0E+02	9.4E+00	1.1E+00
RSD[3] (%)					63.2		161.3		73.8	46.9	76.2		124.1	30.3	33.2	71.2	120.9
NAMC 1-1 A	1	44 × 28	110.0	23.5	1.7E+01	8.2E+04	3.9E+00	1.4E+05	2.7E+03	1.7E+04	<1.0E+00	<9.8E-01	<4.2E-01	<4.9E+02	3.5E+02	1.7E+01	2.1E-01
NAMC 1-1 A	4	53 × 44	108.0	23.2	4.9E+01	7.6E+04	1.7E+01	1.4E+05	5.7E+03	2.2E+04	<4.0E+00	<2.1E+00	1.5E+00	<1.5E+03	3.6E+02	1.5E+01	9.6E-01
NAMC 1-1 A	5	81 × 11	119.5	23.5	1.3E+01	8.2E+04	1.5E+01	1.4E+05	2.7E+03	1.7E+04	<8.5E-01	<5.5E-01	<1.9E-01	<3.4E+02	4.9E+02	1.1E+01	3.9E-01
NAMC 1-1 A	6	44 × 13	129.9	23.5	8.3E+00	8.4E+04	8.8E+00	1.4E+05	3.1E+03	1.3E+04	<1.1E+00	<7.4E-01	<2.4E-01	<3.7E+02	2.7E+02	1.2E+01	5.0E-01
NAMC 1-1 A	7	56 × 22	170.5	23.6	1.5E+01	8.3E+04	8.7E-01	1.4E+05	3.6E+03	1.7E+04	5.9E-01	<2.9E-01	1.9E-01	6.2E+02	5.0E+02	1.2E+01	<2.6E-01
NAMC 1-1 A	8	33 × 29	114.0	23.6	<2.9E+01	7.3E+04	1.1E+02	1.4E+05	1.8E+04	2.1E+04	<7.3E+00	<4.5E+00	1.6E+00	<3.4E+03	3.3E+02	1.1E+01	7.1E-01
NAMC 1-1 A	9	44 × 12	112.0	23.6	4.1E+01	7.7E+04	1.1E+02	1.4E+05	1.2E+04	1.9E+04	<3.9E+00	<2.6E+00	3.1E+00	<1.3E+03	6.9E+02	1.6E+01	1.1E+00
NAMC 1-1 A	10	56 × 23	112.0	23.6	1.3E+01	7.9E+04	5.7E+00	1.4E+05	6.1E+03	2.1E+04	<1.4E+00	<7.0E-01	<2.9E-01	<5.1E+02	4.4E+02	2.7E+01	<5.9E-01
NAMC 1-1 A	11	41 × 17	115.0	23.2	6.8E+01	7.6E+04	9.2E+02	1.4E+05	2.6E+04	1.0E+04	<1.0E+01	<6.4E+00	2.9E+00	<4.3E+03	2.1E+02	9.7E+00	<1.9E+00
NAMC 1-1 A	12	22 × 13	115.0	23.3	<4.9E+01	7.9E+04	2.3E+02	1.4E+05	1.8E+04	1.2E+04	<2.3E+01	<1.8E+01	<1.5E+01	<9.5E+03	2.0E+02	<8.5E+00	<1.6E+00
Mean[3]					2.8E+01		1.4E+02		9.8E+03	1.7E+04			1.9E+00		3.8E+02	1.5E+01	6.5E-01
RSD[3] (%)					77.6		199.0		84.5	24.6			64.5		39.2	37.1	53.2
NAMC 1-2 B	1	26 × 17	111.0	23.5	1.1E+01	7.6E+04	1.1E+01	1.4E+05	5.4E+03	2.5E+04	<3.0E+00	<2.1E+00	<6.3E-01	<1.7E+03	5.6E+02	1.5E+01	6.7E-01
NAMC 1-2 B	2	72 × 18	115.0	22.9	8.8E+00	8.5E+04	7.3E-01	1.4E+05	7.0E+02	8.6E+03	<2.7E-01	1.4E-01	<5.3E-02	1.5E+02	3.1E+02	3.5E+00	<2.1E-02
NAMC 1-2 B	3	44 × 23	103.5	22.9	<9.0E+00	7.8E+04	2.1E+00	1.4E+05	2.3E+03	2.1E+04	<1.3E+00	<1.4E+00	<2.2E-01	5.4E+02	5.8E+02	1.0E+01	1.0E+00
NAMC 1-2 B	5	54 × 31	112.0	23.0	1.8E+01	8.4E+04	1.7E+00	1.4E+05	2.5E+03	1.2E+04	6.1E-01	<2.6E-01	1.2E-01	6.1E+02	4.1E+02	6.6E+00	3.8E-01
NAMC 1-2 B	6	37 × 34	112.0	23.0	2.2E+01	8.1E+04	9.2E-01	1.4E+05	2.9E+03	1.6E+04	3.6E+00	<9.1E-01	9.7E-01	9.1E+02	5.3E+02	8.7E+00	9.1E-01
NAMC 1-2 B	7	54 × 26	127.0	22.2	<4.7E+01	7.8E+04	<7.2E+00	1.3E+05	4.6E+03	1.5E+04	<1.0E+01	<5.9E+00	<2.2E+00	<2.1E+03	1.9E+02	4.6E+00	<7.7E-01
NAMC 1-2 B	9	44 × 12	112.0	23.0	5.7E+01	7.2E+04	<3.4E+00	1.4E+05	1.4E+04	2.2E+04	<5.1E+00	<2.7E+00	<1.2E+00	<9.6E+02	3.3E+02	6.2E+00	1.0E+00
NAMC 1-2 B	10	117 × 16	110.0	23.0	1.2E+02	6.4E+04	8.7E+02	1.4E+05	2.5E+04	2.6E+04	<9.4E+00	<5.8E+00	2.1E+00	<1.7E+03	4.2E+02	1.2E+01	<7.1E-01
Mean[3]					3.9E+01		1.5E+02		7.2E+03	1.8E+04	2.1E+00		1.1E+00	5.5E+02	4.2E+02	8.4E+00	7.9E-01
RSD[3] (%)					107.4		239.5		114.3	35.2	100.2		94.0	57.2	33.1	46.1	33.9
NAMC 1-3	1	65 × 41	98.0	23.2	2.0E+01	7.6E+04	5.6E+02	1.4E+05	6.8E+03	2.2E+04	<1.7E+00	<1.8E+00	6.4E+00	<4.7E+02	4.9E+02	1.6E+01	6.5E-01
NAMC 1-3	2	47 × 23	100.0	23.2	2.0E+01	7.8E+04	7.5E+02	1.4E+05	6.1E+03	2.0E+04	2.7E+00	<2.0E+00	4.2E+00	<5.8E+02	3.2E+02	1.4E+01	7.4E-01
NAMC 1-3	3	55 × 12	100.0	23.2	1.5E+01	7.8E+04	8.8E+02	1.4E+05	4.9E+03	2.0E+04	<3.6E+00	<3.4E+00	<2.7E+00	<1.2E+03	2.7E+02	1.3E+01	1.1E+00
NAMC 1-3	4	41 × 32	100.0	23.3	4.7E+01	6.4E+04	5.0E+01	1.4E+05	5.4E+03	3.9E+04	<4.7E+00	<4.9E+00	1.2E+01	<1.2E+03	5.2E+02	2.6E+01	8.6E-01
NAMC 1-3	5	39 × 28	103.0	23.3	1.5E+01	8.1E+04	6.0E+02	1.4E+05	3.7E+03	1.7E+04	<3.8E+00	<3.6E+00	<3.0E+00	<1.3E+03	2.3E+02	1.0E+01	5.4E-01
NAMC 1-3	6	48 × 16	100.0	23.0	5.7E+01	6.8E+04	8.5E+02	1.4E+05	8.4E+03	3.1E+04	<2.4E+00	<2.6E+00	<1.8E+00	7.8E+02	5.3E+02	2.5E+01	9.2E-01
NAMC 1-3	7	28 × 18	100.0	23.1	<4.0E+01	6.4E+04	2.2E+03	1.4E+05	1.0E+04	3.6E+04	8.2E+00	<3.4E+01	<7.1E+00	<1.6E+03	4.5E+02	2.8E+01	1.4E+00
NAMC 1-3	8	78 × 9	100.0	23.1	6.3E+01	7.2E+04	8.6E+02	1.4E+05	6.7E+03	2.7E+04	<7.7E+00	<8.0E+00	<1.2E+01	<2.2E+03	4.0E+02	1.9E+01	<1.8E+00
Mean[3]					3.4E+01		8.4E+02		6.5E+03	2.7E+04	5.5E+00		7.6E+00		4.0E+02	1.9E+01	8.8E-01
RSD[3] (%)					62.5		71.8		30.5	30.4	71.4		55.3		29.1	35.3	31.9

TABLE 2. *(Cont.)*

Sample ID	Inclusion no.	Size[1] (μm)	T_h (°C)	Salinity[2]	Li	Na	Mg	Cl	K	Ca	Mn	Cu	Zn	Br	Sr	Ba	Pb
Northern Arkansas sphalerite																	
Coarse, pale yellow sphalerite intergrown with finely crystalline quartz																	
NALD 1B-1	1	54 × 18	109.5	19.1	<4.4E+01	5.0E+04	3.2E+03	1.2E+05	1.0E+04	3.2E+04	<6.8E+00			<4.0E+03	1.1E+03	2.4E+01	1.9E+01
NALD 1B-1	2	65 × 23	112.0	19.3	<4.7E+01	6.0E+04	2.1E+03	1.2E+05	<1.0E+03	2.3E+04	<3.3E+01			<1.5E+04	8.0E+02	<2.2E+01	2.4E+02
NALD 1B-1	3	53 × 47	112.0	19.3	<2.7E+01	6.2E+04	1.9E+03	1.2E+05	2.3E+03	2.3E+04	<1.7E+01			<8.1E+03	6.4E+02	2.3E+01	8.5E+01
NALD 1B-1	4	34 × 18	131.4	19.4	<6.1E+01	5.9E+04	2.3E+03	1.2E+05	6.0E+03	2.4E+04	<4.1E+01			<1.6E+04	7.8E+02	<2.5E+01	<4.8E+01
NALD 1B-1	5	88 × 34	127.0	19.3	3.9E+01	5.5E+04	2.9E+03	1.2E+05	7.1E+03	2.9E+04	<1.6E+01			<9.5E+03	9.1E+02	2.4E+01	<3.4E+01
NALD 1B-1	6	31 × 12	126.9	19.4	<1.2E+02	5.7E+04	3.3E+03	1.2E+05	9.5E+03	2.5E+04	<8.7E+01			<2.8E+04	7.3E+02	<3.6E+01	<8.0E+01
NALD 1B-1	7	36 × 28	115.0	19.1	<4.8E+01	5.7E+04	2.1E+03	1.2E+05	7.7E+03	<1.0E+05	<3.0E+01			<1.0E+04	5.3E+02	3.2E+01	3.7E+02
NALD 1B-1	8	124 × 41	115.0	19.5	4.0E+01	5.4E+04	2.4E+03	1.2E+05	6.4E+03	3.1E+04	<6.8E+00			<9.2E+03	9.0E+02	1.6E+01	3.3E+00
NALD 1B-1	9	65 × 18	115.0	19.4	<4.5E+01	6.3E+04	2.2E+03	1.2E+05	3.4E+03	2.1E+04	<3.0E+01			<1.0E+04	5.6E+02	<1.4E+01	6.6E+01
Mean[3]					4.0E+01		2.5E+03		6.5E+03	2.6E+04					7.7E+02	2.4E+01	1.2E+02
RSD[3] (%)					1.4		19.9		41.0	16.0					23.9	24.6	116.6
NALD 1B-2	1	49 × 16	118.1	19.4	3.7E+01	5.0E+04	2.0E+03	1.2E+05	1.3E+04	3.1E+04	<9.0E+00			<7.9E+03	9.6E+02	1.3E+01	3.4E+01
NALD 1B-2	2	81 × 44	115.0	19.9	1.4E+02	6.1E+04	5.3E+02	1.2E+05	<6.2E+03	<1.2E+05	<1.9E+02			<2.3E+04	4.3E+02	<3.1E+02	1.3E+02
NALD 1B-2	3	45 × 41	115.0	19.4	<4.2E+01	5.9E+04	1.2E+03	1.2E+05	<4.2E+04	<1.3E+05	<2.6E+01			<1.6E+04	7.5E+02	1.9E+01	9.9E+01
NALD 1B-2	4	56 × 12	110.0	19.7	2.9E+01	6.7E+04	1.4E+03	1.2E+05	7.2E+03	1.4E+04	<1.2E+01			<8.1E+03	8.4E+02	8.6E+00	1.8E+02
NALD 1B-2	5	54 × 29	118.3	19.0	1.2E+01	6.8E+04	1.1E+03	1.2E+05	2.7E+03	1.1E+04	1.2E+00			<9.0E+02	7.6E+02	6.6E+00	8.6E-01
NALD 1B-2	7	41 × 12	120.0	23.6	<2.5E+01	7.6E+04	1.3E+03	1.4E+05	1.8E+04	1.7E+04	<1.4E+01			<9.8E+03	6.0E+02	2.6E+01	4.5E+01
NALD 1B-2	8	44 × 28	110.0	23.5	1.2E+01	7.5E+04	1.5E+03	1.4E+05	8.8E+03	2.4E+04	5.2E+00			<1.5E+03	1.1E+03	3.3E+01	2.0E+00
Mean[3]					4.6E+01		1.3E+03		9.9E+03	1.9E+04	3.2E+00				7.7E+02	1.7E+01	7.1E+01
RSD[3] (%)					117.9		35.1		58.5	41.0	89.1				28.1	58.9	96.8
Very pale yellow sphalerite																	
NAMC 1-2 A	1	45 × 23	117.3	23.0	4.7E+00	8.1E+04	1.3E+03	1.4E+05	2.4E+03	1.5E+04	8.0E+00			<1.0E+03	3.1E+02	1.4E+01	4.0E+02
NAMC 1-2 A	2	34 × 12	105.0	22.9	9.8E+00	8.0E+04	1.8E+03	1.4E+05	3.3E+03	1.6E+04	1.3E+01			<2.3E+03	6.6E+02	1.5E+01	2.6E+01
NAMC 1-2 A	3	109 × 22	109.0	23.0	8.3E+00	7.7E+04	2.3E+03	1.4E+05	3.7E+03	2.1E+04	1.1E+01			<2.0E+03	4.3E+02	1.5E+01	3.5E+00
NAMC 1-2 A	4	43 × 31	110.0	23.0	<8.9E+00	8.0E+04	2.0E+03	1.4E+05	3.4E+03	1.7E+04	4.7E+00			<2.3E+03	3.7E+02	9.9E+00	1.6E+00
NAMC 1-2 A	5	51 × 26	107.0	23.0	6.6E+00	7.8E+04	2.0E+03	1.4E+05	3.8E+03	2.0E+04	8.1E+00			<2.4E+03	3.9E+02	1.3E+01	6.9E+01
NAMC 1-2 A	6	23 × 19	111.0	23.0	<9.3E+00	8.0E+04	2.0E+03	1.4E+05	3.5E+03	1.8E+04	9.3E+00			<3.8E+03	4.1E+02	1.8E+01	1.0E+01
NAMC 1-2 A	7	21 × 9	110.0	23.0	<2.0E+01	7.7E+04	2.0E+03	1.4E+05	4.9E+03	2.2E+04	<1.3E+01			<7.0E+03	3.9E+02	2.0E+01	2.8E+01
Mean[3]					7.3E+00		1.9E+03		3.5E+03	1.9E+04	9.0E+00				4.2E+02	1.5E+01	7.7E+01
RSD[3] (%)					30.2		16.1		20.8	13.7	31.3				26.5	21.9	187.5
NAMC 1-2 B	1	37 × 23	110.0	23.2	<1.2E+01	7.9E+04	2.0E+03	1.4E+05	3.9E+03	1.9E+04	1.2E+01			<4.8E+03	3.2E+02	8.5E+00	<1.5E+01
NAMC 1-2 B	2	41 × 37	106.2	23.2	<2.9E+01	7.8E+04	2.2E+03	1.4E+05	4.4E+03	2.1E+04	<1.9E+01			<8.8E+03	4.2E+02	1.7E+01	<4.6E+01
NAMC 1-2 B	3	44 × 23	99.2	23.4	1.3E+01	7.6E+04	2.4E+03	1.4E+05	4.7E+03	2.5E+04	1.4E+01			<4.2E+03	4.3E+02	1.4E+01	5.1E+01
NAMC 1-2 B	4	21 × 17	110.0	23.2	<1.8E+01	7.3E+04	2.3E+03	1.4E+05	4.1E+03	2.8E+04	<1.2E+01			<5.3E+03	3.8E+02	1.1E+01	<3.6E+01
NAMC 1-2 B	5	49 × 23	110.0	23.0	1.1E+01	7.4E+04	2.9E+03	1.4E+05	4.2E+03	2.6E+04	2.2E+01			<6.4E+02	6.3E+02	2.0E+01	4.5E+01
Mean[3]					1.2E+01		2.4E+03		4.3E+03	2.4E+04	1.6E+01				4.4E+02	1.4E+01	4.8E+01
RSD[3] (%)					12.0		14.7		7.1	16.2	33.3				27.1	33.0	8.8
Medium-grained disseminated dark yellow-brown sphalerite with associated microcrystalline quartz																	
NAPA 1-1	2	19 × 17	110.0	22.8	<5.0E+01	7.8E+04	1.6E+03	1.4E+05	3.6E+03	1.9E+04	<3.1E+01			<6.0E+03	3.9E+02	<1.0E+02	7.0E+01
Tri-State pink dolomite																	
Medium-grained pink dolomite																	
TSBS 3-5 A	3	23 × 12	114.2	21.1	<1.6E+02	6.3E+04		1.3E+05	1.1E+03			<1.3E+01	<5.3E+00	<4.8E+03	3.4E+02	1.0E+01	1.4E+00
Pale pink crystalline dolomite with a few disseminated sphalerite grains (unspecified location; from University of Iowa collection)																	
TSJ 1 A	2	26 × 23	98.8	22.7	<4.9E+01	7.0E+04		1.4E+05	2.0E+03			<3.5E+00	6.6E+00	3.2E+03	2.0E+02	1.8E+01	9.1E-01

TABLE 2. *(Cont.)*

Sample ID	Inclusion no.	Size[1] (μm)	T_h (°C)	Salinity[2]	Li	Na	Mg	Cl	K	Ca	Mn	Cu	Zn	Br	Sr	Ba	Pb
TSJ 1 E	1	15 × 8	127.2	21.6	<2.3E+02	7.1E+04		1.3E+05	2.4E+03			<1.9E+01	<1.0E+01	<8.0E+03	3.1E+02	<1.7E+02	<9.2E-01
Coarse-grained, vug filling																	
TSWB 2-2 A	1	18 × 15	87.4	16.4	<1.1E+02	5.3E+04		9.9E+04	<3.1E+02			<2.1E+01	1.5E+01	<4.8E+03	9.3E+01	<3.3E+00	<9.2E-01
TSWB 2-2 A	2	20 × 12	115.4	21.8	<2.0E+02	6.3E+04		1.3E+05	<7.1E+02			<3.2E+01	<2.1E+01	<6.5E+03	4.9E+01	<6.9E+00	<3.3E+00
Mean[3]															7.1E+01		
RSD[3] (%)															44.0		
TSWB 2-10 A	1	44 × 23	114.4	23.7	<5.5E+01	7.4E+04		1.4E+05	1.4E+03			6.3E+00	1.3E+01	3.4E+03	3.1E+02	5.9E+00	<1.4E+00
Tri-State quartz																	
Coarse, crystalline quartz with minor finely crystalline																	
TSCV 1-1 A	1	140 × 29	122.2	22.6	<4.4E+01	8.1E+04	1.2E+03	1.4E+05	1.6E+03	1.4E+04	4.5E+00	<2.6E+00	1.5E+00	<9.3E+02	2.5E+02	2.6E+01	6.8E-01
TSCV 1-1 B	1	53 × 15	70.9	23.5	<1.0E+02	8.5E+04	1.2E+03	1.4E+05	1.6E+03	1.2E+04	<3.2E+00	<6.4E+00	2.4E+00	<1.6E+03	2.2E+02	9.1E+00	8.2E-01
TSCV 1-1 B	2	26 × 19	83.0	23.1	<6.6E+01	8.3E+04	3.0E+02	1.4E+05	1.7E+03	1.4E+04	<3.0E+00	<3.5E+00	1.3E+00	<1.5E+03	2.8E+02	1.2E+01	8.3E-01
Mean[3]							7.5E+02		1.6E+03	1.3E+04			1.9E+00		2.5E+02	1.0E+01	8.2E-01
RSD[3] (%)							85.1		3.9	9.7			41.7		17.3	17.0	0.5
TSCV 1-1 C	1	65 × 31	118.0	22.3	<3.9E+01	8.1E+04	<2.9E+01	1.4E+05	1.3E+03	1.2E+04	<1.5E+00	<2.0E+00	<7.6E-01	<7.4E+02	2.1E+02	1.2E+01	8.7E-01
TSCV 1-1 C	2	79 × 35	118.6	22.3	<1.6E+01	8.3E+04	2.8E+01	1.4E+05	1.0E+03	9.1E+03	1.4E+00	<1.1E+00	<3.9E-01	7.1E+02	1.5E+02	9.3E+00	6.9E-01
Mean[3]									1.2E+03	1.1E+04					1.8E+02	1.1E+01	7.8E-01
RSD[3] (%)									18.2	20.6					21.6	20.9	16.3
Coarse, crystalline quartz with minor finely crystalline																	
TSCV 1-2 C	1	23 × 12	142.0	26.2	<5.2E+02	8.1E+04	3.1E+03	1.6E+05	3.0E+03	3.5E+04	<2.5E+01	<4.4E+01	<1.1E+01	<1.5E+04	5.0E+02	1.9E+01	3.0E+00
TSCV 1-2 F	2	15 × 15	200.0	23.6	<1.6E+02	8.2E+04	1.4E+03	1.4E+05	2.5E+03	1.9E+04	<7.9E+00	<1.1E+01	<4.3E+00	<6.2E+03	3.9E+02	1.5E+01	1.3E+00
Fine to medium crystalline quartz																	
TSOR 2-2 A	1	20 × 15	226.7	22.0	<5.6E+02	7.1E+04	1.1E+03	1.3E+05	6.5E+03	2.3E+04	<3.5E+01	<5.1E+01	<2.1E+01	<1.2E+04	3.7E+02	<1.0E+01	<3.0E+00
TSOR 2-2 A	2	23 × 15	150.7	22.3	<6.3E+02	7.3E+04	2.2E+03	1.4E+05	1.1E+04	1.9E+04	<3.0E+01	<5.5E+01	3.4E+01	<1.2E+04	5.7E+02		<5.8E+01
Mean[3]							1.7E+03		8.7E+03	2.1E+04					4.7E+02		
RSD[3] (%)							43.9		35.6	12.3					30.0		
TSOR 2-2 B	2	53 × 35	91.0	23.0	<7.8E+01	7.8E+04	1.8E+03	1.4E+05	2.1E+03	2.1E+04	5.0E+00	<6.6E+00	<3.5E+00	<1.7E+03	3.7E+02	1.8E+01	1.1E+00
TSOR 2-2 B	3	41 × 35	90.2	22.5	<2.4E+02	7.4E+04	2.1E+03	1.4E+05	2.2E+03	2.4E+04	<1.2E+01	<2.1E+01	<9.7E+00	<3.9E+03	5.6E+02	2.1E+01	<1.7E+00
TSOR 2-2 B	4	44 × 18	80.7	22.4	<1.2E+02	7.9E+04	1.6E+03	1.4E+05	2.4E+03	1.5E+04	6.2E+00	<7.1E+02	<1.5E+01	<1.9E+03	6.3E+02	1.6E+01	<6.7E+00
Mean[3]							1.8E+03		2.2E+03	2.0E+04	5.6E+00				5.2E+02	1.8E+01	
RSD[3] (%)							14.1		6.1	21.5	13.9				25.6	14.8	
TSOR 2-2 D	2	38 × 18		22.1	<8.6E+01	7.9E+04	1.3E+03	1.3E+05	1.0E+03	1.4E+04	<7.9E+00	<9.4E+00	<4.1E+00	<2.9E+03	2.8E+02	1.3E+01	<8.6E-01
Medium-coarse crystalline quartz																	
TSPC 1-1 A	1	74 × 45	51.0	16.0	3.1E+01	5.5E+04	8.0E+02	9.7E+04		1.2E+04	<1.5E+01	<2.2E+00	<1.1E+00	<1.4E+03	3.3E+02	7.3E+00	<8.4E-01
TSPC 1-1 A	2	12 × 9	57.2	16.0	3.5E+01	5.6E+04	5.3E+02	9.7E+04		1.0E+04	<1.6E+01	<4.8E+00	<2.5E+00	<3.7E+03	3.4E+02	1.0E+01	<3.1E+00
TSPC 1-1 A	3	18 × 12	59.7	15.8	<3.6E+01	5.6E+04	1.2E+03	9.6E+04		9.5E+03	<4.3E+01	<1.3E+01	<7.8E+00	<7.2E+03	4.5E+02	1.2E+01	<4.8E+00
TSPC 1-1 A	4	18 × 12	63.3	16.0	2.8E+01	5.7E+04	9.5E+02	1.1E+05		1.1E+04	<3.8E+01	<1.1E+01	<5.8E+00	<5.8E+03	3.4E+02	1.1E+01	<4.5E+00
TSPC 1-1 A	5	20 × 18	57.2	16.0	8.3E+00	5.2E+04	1.4E+03	1.1E+05	1.5E+03	1.9E+04	<9.1E+00	<2.8E+00	<1.7E+00	<1.4E+03	6.5E+02	1.5E+01	<9.2E-01
Mean[3]					2.6E+01		9.7E+02			1.2E+04					4.2E+02	1.1E+01	
RSD[3] (%)					46.1		34.4			30.9					32.8	26.5	
TSWC 1-2 B	3	35 × 15	103.6	23.3	<3.1E+01	8.2E+04	3.1E+02	1.4E+05	2.1E+03	1.6E+04	<2.0E+00	<3.7E+00	<1.7E+00	<1.9E+03	5.5E+02	1.6E+01	<1.2E+00

TABLE 2. *(Cont.)*

Sample ID	Inclusion no.	Size[1] (μm)	T_h (°C)	Salinity[2]	Li	Na	Mg	Cl	K	Ca	Mn	Cu	Zn	Br	Sr	Ba	Pb
TSWC 1-2 D	2	91 × 58	121.8	24.3	1.0E+01	8.6E+04	1.3E+03	1.5E+05	2.3E+03	1.6E+04	4.0E+00	<4.4E-01	2.5E+00	6.7E+02	5.5E+02	1.4E+01	1.2E+00
TSWC 1-2 E	1	26 × 20	100.7	24.7	<2.5E+01	8.8E+04	1.4E+03	1.5E+05	1.8E+03	1.6E+04	3.9E+00	<2.0E+00	1.8E+00	<1.3E+03	7.1E+02	1.5E+01	7.7E-01
TSWC 1-2 E	2	47 × 44	67.8	23.8	<5.3E+01	8.2E+04	1.4E+03	1.4E+05	2.4E+03	1.9E+04	4.7E+00	<4.0E+00	5.0E+00	<3.0E+03	7.4E+02	2.6E+01	2.5E+00
Mean[3]							1.4E+03		2.1E+03	1.7E+04	4.3E+00		3.4E+00		7.3E+02	2.0E+01	1.6E+00
RSD[3] (%)							0.5		21.0	10.5	13.5		66.2		2.5	38.0	74.4
TSWC 1-2 G	1	131 × 15	105.3	24.4	<7.9E+01	8.6E+04	2.1E+03	1.5E+05	2.1E+03	1.7E+04	5.7E+00	<6.4E+00	3.7E+00	<3.1E+03	3.7E+02	1.2E+01	1.4E+00
TSWC 1-2 G	2	131 × 44	102.0	24.3	<1.5E+01	8.6E+04	1.1E+03	1.5E+05	2.2E+03	1.6E+04	4.0E+00	<1.3E+00	1.8E+00	7.7E+02	5.0E+02	1.3E+01	1.2E+00
Mean[3]							1.6E+03		2.1E+03	1.7E+04	4.8E+00		2.8E+00		4.4E+02	1.2E+01	1.3E+00
RSD[3] (%)							43.2		5.4	4.4	26.1		49.0		20.2	8.4	9.2
TSWC 1-4 C	2	20 × 15	86.4	16.0	<1.2E+01	5.6E+04	1.0E+03	1.3E+05	2.4E+03	1.5E+04	<7.3E+00	<2.4E+00	<1.6E+00	<1.5E_03	5.2E+02	1.0E+01	<1.0E+00
TSWC 1-4 C	3	18 × 9	85.5	16.0	<2.7E+01	5.6E+04	1.0E+03	1.3E+05	2.3E+03	1.5E+04	<2.5E+01	<6.9E+00	<4.0E+00	<4.3E_03	5.2E+02	8.2E+00	<2.7E+00
TSWC 1-4 C	4	26 × 23	88.5	15.8	<4.7E+00	5.5E+04	9.7E+02	1.3E+05	2.8E+03	1.5E+04	<5.2E+00	<1.5E+00	1.9E+00	<8.0E+02	5.4E+02	9.4E+00	<6.3E-01
TSWC 1-4 C	5	20 × 9	91.5	16.0	<9.1E+00	5.5E+04	1.1E+03	1.3E+05	2.5E+03	1.8E+04	<1.0E+01	<3.7E+00	<1.8E+00	<1.8E+03	7.0E+02	1.2E+01	<1.1E+00
TSWC 1-4 C	6	50 × 29	89.3	16.0	<6.6E+00	5.7E+04	8.7E+02	1.3E+05	2.5E+03	1.2E+04	<6.0E+00	<1.5E+00	<1.2E+00	<7.7E+02	4.8E+02	1.0E+01	<5.7E-01
Mean[3]							1.0E+03		2.5E+03	1.5E+04					5.5E+02	9.9E+00	
RSD[3] (%)							9.7		7.4	14.2					15.3	13.0	
Tri-State sphalerite																	
Coarse-grained, pale yellow sphalerite																	
TSBS 1-7 A	1	23 × 18	115.3	20.4	<7.6E+02	7.0E+04	9.7E+02	1.2E+05		1.7E+04	<3.4E+01			<1.1E+04	2.1E+02	6.5E+00	2.7E+01
TSBS 1-7 B	1	53 × 30	101.7	19.8	6.5E+01	7.1E+04	1.2E+03	1.2E+05	1.5E+03	1.2E+04	4.4E+00			2.7E+03	3.6E+02	6.9E+00	<6.0E-01
TSBS 1-7 B	2	35 × 30	95.7	19.6	<2.8E+02	6.5E+04	2.1E+03	1.2E+05	2.4E+03	2.0E+04	<1.3E+01			<6.7E+03	5.8E+02	1.3E+01	7.9E+00
TSBS 1-7 B	3	41 × 30	111.4	19.6	<1.6E+02	6.8E+04	1.4E+03	1.2E+05	1.6E+03	1.5E+04	9.5E+00			<2.6E+03	4.8E+02	7.8E+00	<8.6E-01
Mean[3]							1.6E+03		1.8E+03	1.6E+04	7.0E+00				4.7E+02	9.3E+00	
RSD[3] (%)							32.6		28.8	28.4	52.3				23.6	37.2	
TSBS 1-7 D	1	117 × 53	103.0	18.5	2.8E+01	6.5E+04	1.2E+03	1.1E+05	1.4E+03	1.2E+04	4.9E+00			3.0E+03	6.0E+02	1.0E+01	<1.9E+01
TSBS 1-7 D	2	117 × 44	105.0	19.1	<2.4E+01	6.8E+04	1.3E+03	1.2E+05	1.8E+03	1.3E+04	3.2E+00			2.7E+03	6.1E+02	7.7E+00	<3.7E+00
Mean[3]							1.2E+03		1.6E+03	1.3E+04	4.0E+00			2.9E+03	6.0E+02	9.0E+00	
RSD[3] (%)							1.9		16.0	2.8	28.7			7.7	0.9	20.9	
Coarse-grained, pale yellow sphalerite																	
TSBS 4-5 A	1	26 × 15	93.9	18.2	2.0E+01	6.3E+04	2.0E+03	1.1E+05	2.1E+03	1.3E+04	1.3E+01			<2.5E+03	3.8E+02	1.1E+01	1.5E+01
TSBS 4-5 A	2	41 × 26	94.3	17.7	8.7E+00	6.0E+04	1.6E+03	1.1E+05	3.0E+03	1.6E+04	<1.0E+01			<3.5E+03	5.4E+02	1.1E+01	<2.2E+01
TSBS 4-5 A	4	58 × 29	88.7	18.5	1.4E+01	6.3E+04	1.2E+03	1.1E+05	3.4E+03	1.5E+04	6.4E+00			<1.3E+03	6.8E+02	<3.6E+01	2.6E+00
Mean[3]					1.4E+01		1.6E+03		2.8E+03	1.5E+04	9.5E+00				5.3E+02	1.1E+01	9.0E+00
RSD[3] (%)					38.8		25.2		22.8	7.6	46.9				29.0	2.1	100.5
Coarse-grained, pale yellow sphalerite																	
TSBS 4-6 A	2	23 × 12	93.2	18.8	<3.0E+01	6.2E+04	1.0E+03	1.1E+05	9.2E+03	1.4E+04	<3.0E+01			<1.3E+04	4.6E+02	1.6E+01	2.3E+01
TSBS 4-6 A	3	18 × 15	103.8	21.3	<2.4E+01	7.5E+04	1.3E+03	1.3E+05		1.5E+04	<2.8E+01			<9.2E+03	5.5E+02	1.1E+01	9.5E+01
TSBS 4-6 A	5	24 × 19	100.0	19.1	1.1E+01	6.4E+04	1.2E+03	1.1E+05	6.3E+03	1.6E+04	5.1E+00			<1.2E+03	5.7E+02	1.4E+01	1.4E+00
TSBS 4-6 A	7	32 × 28	100.0	19.1	<1.3E+01	6.4E+04	1.3E+03	1.1E+05	2.6E+03	1.7E+04	<1.4E+01			<5.1E+03	5.0E+02	1.5E+01	3.0E+00
TSBS 4-6 A	8	44 × 17	100.0	19.1	1.9E+01	6.2E+04	1.4E+03	1.1E+05	3.7E+03	2.0E+04	<8.9E+00			<8.7E+03	5.3E+02	1.4E+01	7.7E+00
TSBS 4-6 A	9	31 × 25	100.0	19.1	1.5E+01	6.6E+04	1.2E+03	1.1E+05	2.5E+03	1.4E+04	1.7E+01			<3.8E+03	4.4E+02	1.8E+01	1.4E+01
TSBS 4-6 A	10	54 × 12	100.0	19.1	<4.9E+00	7.0E+04	5.8E+02	1.1E+05	1.1E+03	8.5E+03	<4.3E+00			<1.8E_03	2.1E+02	4.5E+00	5.0E+00
Mean[3]					1.5E+01		1.1E+03		4.2E+03	1.5E+04	1.1E+01				4.7E+02	1.3E+01	2.1E+01
RSD[3] (%)					26.8		24.1		71.1	23.0	74.9				25.9	32.8	156.8

TABLE 2. *(Cont.)*

Sample ID	Inclusion no.	Size[1] (μm)	T_h (°C)	Salinity[2]	Li	Na	Mg	Cl	K	Ca	Mn	Cu	Zn	Br	Sr	Ba	Pb
Coarse, medium yellow sphalerite																	
TSOR 2-3 A	2	29 × 23	105.2	23.3	<1.2E+02	8.5E+04	1.2E+03	1.4E+05	1.3E+03	1.2E+04	1.4E+01			3.3E+03	1.9E+02	6.0E+00	<6.6E-01
TSOR 2-3 A	3	44 × 23	98.7	23.6	<1.1E+02	8.6E+04	1.4E+03	1.4E+05	1.5E+03	1.2E+04	1.8E+01			3.7E+03	1.8E+02	6.3E+00	1.3E+00
TSOR 2-3 A	4	23 × 20	100.2	23.2	<2.5E+02	8.5E+04	1.5E+03	1.4E+05	1.7E+03	1.2E+04	<1.3E+01			<6.1E+03	3.1E+02	7.1E+00	<8.4E-01
TSOR 2-3 A	5	23 × 18	98.9	23.5	<1.4E+02	8.6E+04	1.1E+03	1.4E+05	1.4E+03	1.1E+04	<8.0E+00			<2.2E+03	1.6E+02	8.9E+00	<6.8E-01
Mean[3]							1.3E+03		1.5E+03	1.2E+04	1.6E+01			3.5E+03	2.1E+02	7.1E+00	
RSD[3] (%)							11.5		10.8	6.2	14.0			8.7	32.0	18.6	
Medium-grained dark yellow-brown sphalerite																	
TSPC 2-1 A	1	43 × 18	97.9	23.0	<2.4E+02	8.1E+04	1.2E+03	1.3E+05	1.3E+03	1.6E+04	<1.4E+01			<4.0E+03	2.6E+02	7.2E+00	<1.6E+00
TSPC 2-1 B	1	93 × 29	119.9	23.6	<1.6E+02	8.5E+04	1.2E+03	1.4E+05	1.7E+03	1.3E+04	<8.0E+00			<3.2E+03	2.4E+02	1.4E+01	1.5E+00
Coarse, dark reddish brown sphalerite																	
TSWB 3-11 D	3	32 × 29	106.5	24.1	1.5E+01	7.9E+04	1.4E+03	1.5E+05		2.6E+04	<5.8E+00			<2.3E+03	6.2E+02	4.0E+01	1.1E+00

Note: Zn and Cu values are not reported for sphalerite-hosted fluid inclusions and Ca, Mg, and Mn values are not reported for dolomite-hosted fluid inclusions because of matrix interferences from the mineral host

[1] Size is expressed as the longest overall part of the fluid inclusion by the longest part orthogonal to it

[2] Salinity is expressed as wt percent NaCl equivalent and was computed using the equation of state of Bodnar (1993)

[3] Mean and relative standard deviation (RSD) values are computed for each element in each fluid inclusion group measured by LA-ICP-MS where two or more measurements were obtained.

TABLE 3. Summary of Microthermometric Data on Fluid Inclusions from the Tri-State and Northern Arkansas Districts

Host[1]	T_h (°C)	Salinity[2]	Size[3] (μm)
Tri-State			
Sphalerite[23]	101.4 (7.1)	20.5 (2.1)	45 × 24
Quartz[29]	100.9 (40.6)	20.8 (3.7)	47 × 23
Dolomite[6]	109.6 (14.1)	21.2 (2.5)	38 × 17
N. Arkansas			
Sphalerite[33]	112.9 (6.7)	21.5 (1.8)	50 × 24
Quartz[35]	113.1 (12.8)	23.1 (0.3)	50 × 22

Note: Numbers in parentheses are 1σ

[1] Numbers in superscript refer to the number of inclusions analyzed in that host mineral

[2] Mean of salinity, estimated from microthermometric data using low-temperature phase equilibria in the NaCl-H_2O model system and expressed as wt percent NaCl equiv

[3] Refers to the sizes in the two observed dimensions

hosts fluid inclusions that have the largest range of fluid homogenization temperatures and salinities. Pink dolomite, which began precipitating after quartz and has a relatively narrow paragenetic distribution, hosts fluid inclusions that have primarily transitional properties. Sphalerite, which began precipitating after pink dolomite and quartz and has a broad paragenetic distribution similar to that of quartz, hosts

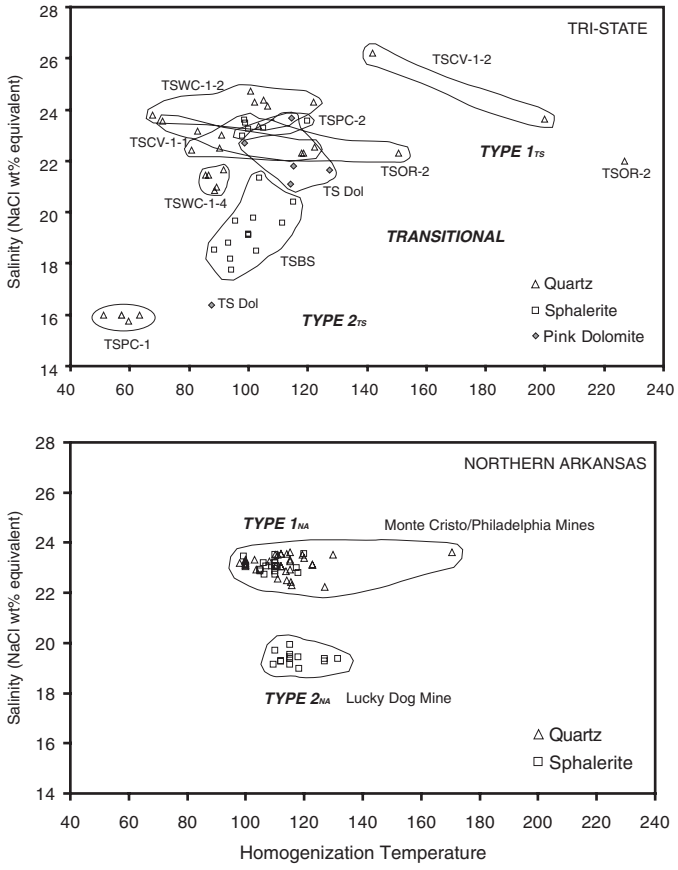

FIG. 4. Temperature of homogenization vs. salinity for fluid inclusions from the Tri-State and Northern Arkansas districts. Solid lines enclose results from individual samples and the different host minerals are indicated by different symbols.

TABLE 4. Summary of the Different Fluid Types in the Tri-State and Northern Arkansas Districts Identified by Fluid Inclusion Microthermometry

District	Fluid types identified	Comment
Tri-State	Type 1_{TS}	High-salinity (>21 wt % NaCl equiv) fluids preserved in both quartz, sphalerite, and pink dolomite
	Type 2_{TS}	Lower salinity (~16 wt % NaCl equiv) quartz-hosted inclusions of sample TSPC-1
	Transitional	Fluids of intermediate salinity (~17.5–21 wt % NaCl equiv) trapped in the three TSBS samples
N. Arkansas	Type 1_{NA}	High-salinity (~23 wt % NaCl equiv) fluids preserved in both quartz and sphalerite from the Monte Cristo and Philadelphia mines of the Rush Creek subdistrict
	Type 2_{NA}	Lower salinity (~18–20 wt % NaCl equiv) fluids hosted in sphalerite from the Lucky Dog mine of the Tomahawk Creek subdistrict

fluid inclusions with mainly transitional properties that overlap fluid inclusions hosted by pink dolomite but extend to lower homogenization temperatures and salinities than most of the pink dolomite-hosted fluid inclusions.

In fluid inclusions in samples from the Northern Arkansas district, the microthermometric data define two distinct fluid groups. Samples of both sphalerite and quartz from the Monte Cristo and Philadelphia mines of the Rush Creek subdistrict (hereafter "type 1_{NA}" fluids) host inclusions with a relatively narrow range of fluid salinities; averages for sphalerite and quartz are 23.0 and 23.1 wt percent NaCl equiv, respectively, with mean homogenization temperatures of 109.0° and 113.1°C. Sphalerite samples from the Lucky Dog mine of the Tomahawk Creek subdistrict show a broadly similar mean homogenization temperature of 117°C but a lower mean salinity of 19.9 wt percent NaCl equiv (hereafter "type 2_{NA}" fluids). The limited spread in the microthermometric data, in particular the fluid salinities, from the two different northern Arkansas subdistricts suggests that little mixing occurred between the fluids at each of these locations unless it involved fluids of very similar temperature and salinity at each location.

LA-ICP-MS results

The following section presents the much greater range of chemical information provided by LA-ICP-MS analysis. In particular, the key question is examined of whether the inferred ore-forming fluid, which precipitated and subsequently became trapped within sphalerite, displays any significant geochemical differences to the fluid responsible for precipitating the gangue phases, despite having very similar microthermometric properties in both the type 1_{TS} and type 1_{NA} fluids.

In total, 65 inclusion analyses were attempted on samples from the Tri-State district, and useable signals (i.e., those yielding elemental data above detection for at least six elements) were derived from 52 inclusions. In the samples from the Northern Arkansas district, 68 inclusion analyses yielded useable signals from a total of 82 attempted. The most common reason for an unsuccessful analysis was insufficient inclusion volume giving poor limits of detection. In both districts the elements consistently determined were Li, Mg, Cl, K, Ca, Mn, Cu, Zn, Sr, Ba, and Pb. The elements Cr, Fe, Co, Ni, Cu, Br, Mo, Ag, and Au were below detection in most inclusions and, with the exception of Br, are not reported. Na was estimated using measured element/Cl ratios and an empirical formula that relates the weight percent NaCl equiv to the sum of the concentrations of the major chloride species in solution (cf. Heinrich et al., 2003).

Uncertainty in the LA-ICP-MS analyses can be partly assessed by computing standard deviations for groups of fluid inclusions representing the same inferred fluid type (Tables 5, 6). Relative standard deviation values for laser-determined element concentrations are mostly in the range of 7 to 57 percent for Tri-State fluid groups, broadly in line with previous studies (e.g., Stoffell et al., 2004). Relative standard deviation values for northern Arkansas fluid groups are generally higher, mostly in the range of 24 to 89 percent. The higher values are in part due to the larger number of analyses from which they were calculated but mainly because the inclusions within each group appear to be recording significant local variation in fluid composition (see discussion below), despite consistent microthermometric properties, that are not observed in the Tri-State district.

Major and minor elements

A detailed listing of the LA-ICP-MS results is presented in Table 2, and the results are summarized in Tables 5 and 6, which are subdivided according to the fluid types identified from the microthermometric data. In the samples from the Tri-State district, the higher salinity and higher T_h (type 1_{TS}) fluids trapped in quartz have a markedly higher Ca content than the lower salinity and lower T_h (type 2_{TS}) quartz-hosted fluids (16,900 compared to 12,300 ppm). Of the fluids trapped in sphalerite from the Tri-State district, both type 1_{TS} and the transitional fluids have very similar average Ca contents of 14,500 to 15,000 ppm. In addition, there is no systematic variation of Ca concentration with chloride content in the TSBS fluids. Mg is present at similar concentrations (1,300–1,400 ppm) in both quartz and sphalerite-hosted type 1_{TS} inclusions, and also in the transitional fluid trapped by the TSBS sphalerite samples, whereas the lower salinity type 2_{TS} fluid in quartz has a lower average Mg content of 970 ppm. The mean K content of the type 1_{TS} inclusions in quartz is 2,630 ppm, higher than the type 1_{TS} fluid in sphalerite, which averages 1,480 ppm. A single analysis suggests K concentrations may also be low in the type 2_{TS}, lower salinity fluid hosted in quartz (~1,550 ppm), although the highest mean concentrations are recorded in the fluid inclusions of transitional salinity from TSBS (3,010 ppm). Inclusions in pink dolomite have an average K concentration of 1,720 ppm.

A further important chemical distinction between fluid types is a contrast in Br content. Three quartz-hosted inclusions of type 1_{TS} gave an average Br concentration of 715 ppm, in contrast to much higher Br concentrations recorded in both type1_{TS} and type 2_{TS} sphalerite-hosted inclusions (3,490 and 2,810 ppm, respectively). As a cautionary note, this

TABLE 5. Summary of Mean Compositional Data (ppm) from Fluid Inclusions Hosted by Quartz, Sphalerite, and Pink Dolomite from the Tri-State District and Comparison with Contemporary Basinal Brines

Element	Quartz Type 1 High salinity	1σ	Sphalerite Type 1 High salinity	1σ	Quartz Type 2 Lower salinity	1σ	Sphalerite Trans. salinity	1σ	Pink Dolomite Type 1	1σ	Oil field brines[3]
Cl[1]	132,306[24]	16,610	141,641[7]	3,858	100,302[5]	5,049	115,879[16]	5,344	128,733[6]	15,355	132,000
Na[2]	75,817[24]	11,156	83,785[7]	2,750	55,380[5]	1,729	66,121[16]	6,515	65,805[6]	7,747	49,700
Ca	16,885[24]	5,161	14,561[7]	5,469	12,284[5]	3,791	14,864[16]	2,960	n.d.	n.d.	26,800
K	2,627[24]	2,035	1,483[6]	177	1,547[1]	n.d.	3,046[14]	2,210	1,724[4]	559	1,870
Br	715[3]	49	3,488[2]	304	n.d.	n.d.	2,814[3]	198	n.d.	n.d.	n.d.
Sr	457[24]	166	279[7]	159	421[5]	138	481[16]	135	217[6]	123	1,340
Mg	1,308[23]	674	1,289[7]	132	967[5]	333	1,310[16]	371	n.d.	n.d.	2,030
Li	10.5[1]	n.d.	15.1[1]	n.d.	25.6[4]	11.8	18.1[8]	19.0	n.d.	n.d.	n.d.
Mn	4.4[9]	1.4	16.1[2]	2.0	n.d.	n.d.	7.9[8]	5.0	n.d.	n.d.	n.d.
Pb	1.3[13]	0.7	1.3[3]	0.2	n.d.	n.d.	18.3[11]	27	1.2[2]	0.3	20
Zn	5.6[10]	9.9	n.d.	n.d.	n.d.	n.d.	n.d.	n.d.	11.5[3]	4.3	100
Ba	14.3[22]	5.0	12.8[7]	12.0	11.0[5]	2.9	11.1[15]	4.0	11.5[3]	6.2	43

Notes: Superscripts following mean elemental concentrations indicate the number of values from which the mean value was calculated; n.d. = not determined
[1] Cl values estimated from microthermometric data, using low-temperature phase equilibria in the NaCl-H_2O model system (Bodnar, 1993)
[2] Na values corrected for other cations as described in the text
[3] Mean of data reported by Carpenter et al. (1974); the elements Cr, Fe, Co, Ni, Cu, Br, Mo, Ag, and Au were all below detection in the majority of inclusions

pattern is based on a relatively small number of large inclusions (three in quartz and five in sphalerite) that yielded Br concentrations above the instrumental detection limit. The data nonetheless point to a consistent, marked difference in fluid chemistry based on quantifiable responses to both Br and Cl (e.g., Fig. 5).

Ba concentrations in the Tri-State fluids are relatively uniform, with the vast majority ranging from 5 to 25 ppm in type 1_{TS} fluids trapped in quartz, sphalerite, and dolomite, and a very similar range observed in the type 2_{TS} fluids. The majority of Sr concentrations fall in the same range (100–700 ppm) for all fluid types, with averages of 400 to 500 ppm. The mean Sr concentration of pink dolomite-hosted inclusions is lower (220 ppm), but this is principally due to two anomalously low analyses of <100 ppm Sr. Li was only detected in two inclusions of the type 1_{TS} fluid, one in quartz (10 ppm) and one in sphalerite (15 ppm). In the type 2_{TS} fluid in quartz, the mean Li concentration is 26 ppm, and the transitional, sphalerite-hosted fluids have a mean Li concentration of 18 ppm. Mn concentrations are also uniformly low, typically <10 ppm and not exceeding 18 ppm in any of the fluids analyzed from the Tri-State district.

In northern Arkansas, the higher salinity type 1_{NA} sphalerite- and quartz-hosted inclusions also both show a fairly uniform Ca concentration of around 19,000 ppm, whereas the lower salinity type 2_{NA} fluid from the Lucky Dog mine records higher Ca concentrations of around 23,500 ppm. Both the type 1_{NA} and type 2_{NA} sphalerite-hosted inclusions

FIG. 5. Transient (a) Cl and (b) Br signal responses for LA-ICP-MS analysis of a quartz-hosted fluid inclusion (91 × 58 μm), sample TSWC 1-2 D inclusion 2, from Tri-State (670 ppm Br).

TABLE 6. Summary of Mean Compositional Data (ppm) from Fluid Inclusions Hosted by Quartz and Sphalerite from the Northern Arkansas District and Comparison with Contemporary Basinal Brines

Element	Quartz Type 1 Monte Cristo and Philadelphia mines	1σ	Sphalerite Type 1 Monte Cristo and Philadelphia mines	1σ	Sphalerite Type 2 Lucky Dog mine	1σ	Oil field brines[3]
Cl[1]	140,410[35]	2,250	139,541[17]	1,200	120,710[16]	8,739	132,000
Na[2]	77,160[35]	6,515	77,309[17]	3,038	60,717[16]	7,661	49,700
Ca	19,205[35]	7,602	19,103[17]	4,661	23,521[13]	6,519	26,800
K	7,077[35]	6,270	6,211[17]	5,027	7,837[13]	4,272	1,870
Br	513[10]	282	n.d.	n.d.	n.d.	n.d.	n.d.
Sr	412[35]	148	407[17]	107	773.5[16]	193	1,340
Mg	324[33]	490	1,942[17]	479	1,970[16]	772	2,030
Li	30.5[31]	24.7	10.9[7]	5.9	44.4[7]	44.7	n.d.
Mn	2.05[10]	2.42	11.2[9]	4.8	3.2[2]	2.8	n.d.
Pb	0.83[24]	0.65	66.3[11]	112.9	93.6[14]	106	20
Zn	2.82[15]	3.21	n.d.	n.d.	n.d.	n.d.	100
Ba	12.8[35]	6.8	14.4[16]	3.8	20.3[11]	8.8	43

Notes: Superscripts following mean elemental concentrations indicate the number of values from which the mean value was calculated; n.d. = not determined

[1] Cl values estimated from microthermometric data, using low-temperature phase equilibria in the $NaCl\text{-}CaCl_2\text{-}H_2O$ model system (Oakes et al., 1992)

[2] Na values estimated as described in the text

[3] Mean of data reported by Carpenter et. al. (1974); the elements Cr, Fe, Co, Ni, Cu, Br, Mo, Ag, and Au were all below detection in the majority of inclusions

have elevated Mg concentrations relative to Tri-State, with an average of 1,940 to 1,970 ppm. In contrast, the high-salinity type 1_{NA} fluids in quartz record much lower Mg concentrations, having an average of just 320 ppm. Potassium concentrations are significantly higher than in type 1_{NA} fluids trapped in both quartz (7,080 ppm) and sphalerite (6,210 ppm) and in the type 2_{NA} fluid trapped in sphalerite (7,840 ppm). As observed in the samples from the Tri-State district, the Br concentration of type1_{NA} quartz-hosted inclusions is low, with a mean value of 510 ppm (based on 10 analyses). Br was not detected in either the type 1_{NA} or type 2_{NA} sphalerite-hosted inclusions.

The range of Ba concentrations in samples from the Northern Arkansas district is very similar to that observed in samples from the Tri-State district, mostly around 5 to 25 ppm in all fluid types. Strontium concentrations are again similar in the different fluid types, with the majority of analyses in both quartz- and sphalerite-hosted type1_{NA} fluids in the range 200 to 600 ppm and mean concentrations of ~410 ppm. The lower salinity type 2_{NA} fluids from the Lucky Dog mine showed slightly elevated Sr concentrations, ranging from 400 to 1,000 ppm with an average of 770 ppm. Lithium is present at an average of 30 ppm in quartz-hosted type 1_{NA} fluids and at slightly lower concentrations (11 ppm) in type 1_{NA} sphalerite-hosted fluids. Type 2_{NA} fluids in sphalerite from the Lucky Dog mine contain an average of 44 ppm. Mn concentrations, as observed in samples from the Tri-State district, are uniformly low (typically <10 ppm).

It is pertinent to note here that although providing useful constraints on the absolute concentrations of Li and Mn in the fluids involved in gangue and ore mineral precipitation, when the error associated with the characterization of Li and Mn in fluid inclusions is considered (Stoffell, 2008) none of the variations in the concentrations of these two elements observed in this study are considered to be significant.

Ore metals

Concentrations of zinc in the type 1_{TS} fluids trapped in pink dolomite and quartz from the Tri-State district are relatively low, typically on the order of a few ppm with one higher value of a few tens of ppm (Fig. 6). No Zn was detected in the type 2_{TS} fluids hosted by quartz, although detection limits varied from 1 to 8 ppm. These values are within the range recorded for modern basinal brines, although generally lower than for the metal-rich brines reported by Carpenter et al. (1974) and shown in Figure 6, implying that these fluids were not anomalously Zn rich. It should be noted that obtaining Zn values for either type 1_{TS} or type 2_{TS} sphalerite-hosted fluid inclusions is not possible due to the interference from the mineral matrix, although, given that the fluid was evidently saturated with respect to sphalerite at this

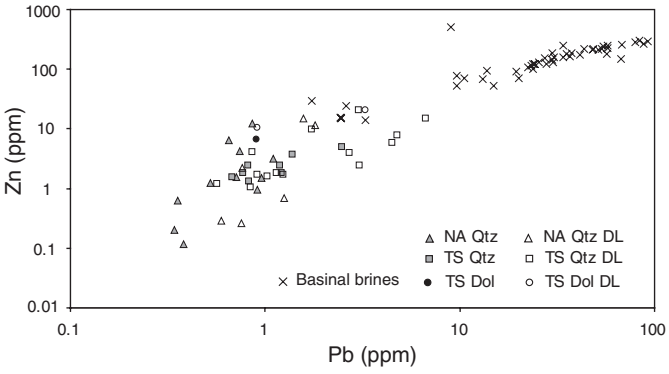

FIG. 6. Pb and Zn concentrations of fluids trapped in quartz from the Tri-State and Northern Arkansas districts compared to concentrations measured in modern basinal brines (Carpenter et al., 1974). Note consistent trajectory between the two datasets. DL = detection limit, representing maximum possible concentrations.

point, fluid Zn concentrations are likely to have been much higher than those recorded in the quartz-hosted fluids, possibly up to ~1,000 ppm (see below).

Lead concentrations in the type 1_{TS} inclusions in pink dolomite and quartz are somewhat lower on average than the Zn concentrations in these fluids, ranging from a few tenths of a ppm to around 3 ppm. As for Zn, no Pb was detected in the type 2_{TS} inclusions hosted by quartz (detection limits ranged from 0.8–4.8 ppm). Where both metals were detected in the quartz-hosted type 1_{TS} fluid, Zn/Pb ratios (by mass) display a narrow range of 1.5 to 3. Two analyses of dolomite-hosted inclusions yielded 0.9 and 1.4 ppm Pb and three yielded Zn concentrations of 6.6 to 14.5 ppm, with one analysis of both Zn and Pb giving a ratio of 7.3. Sphalerite-hosted inclusions have significantly higher Pb concentrations (Tables 5, 6) of up to 95 ppm, with those of transitional salinity having the highest concentrations (the mean for this group is 18 ppm). Limited data (n = 3) suggest that the type 1_{TS} fluids trapped in sphalerite have lower Pb concentrations (1.1–1.5 ppm), but it is possible that these are secondary inclusions that trapped the same fluid as that hosted by quartz and dolomite. Overall, there is a clear distinction between the range of Pb concentrations in inclusions hosted by sphalerite and that of inclusions hosted by gangue (Fig. 7).

In northern Arkansas, Zn concentrations in type 1_{NA} quartz-hosted inclusions vary over two orders of magnitude, from a few tenths of a ppm to around 12 ppm, again well below the maximum recorded concentrations in modern sedimentary brines (Fig. 6). The Pb concentration of these fluids is low, averaging 0.8 ppm. Zn/Pb ratios are more variable than those from Tri-State, ranging from <1 to ~10, but with a similar mean of 3.4.

Both the type 1_{NA} and type 2_{NA} fluids trapped in sphalerite have significantly elevated Pb concentrations, reaching nearly 400 ppm in both fluids and having mean concentrations of 66 and 94 ppm, respectively. The distinction between the Pb concentration of the fluids trapped in sphalerite and that trapped in gangue is even more marked in the Northern Arkansas than in the Tri-State district (Fig. 7).

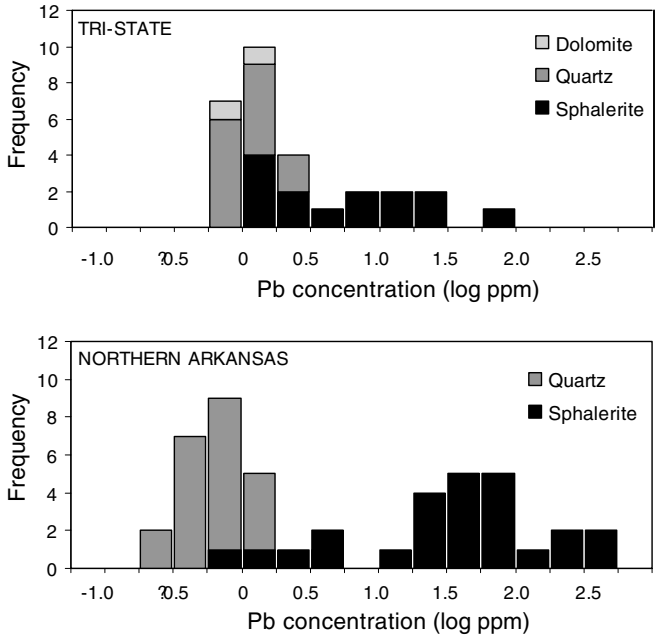

FIG. 7. Frequency histograms comparing Pb concentrations in inclusions hosted by gangue and sphalerite from the Tri-State and Northern Arkansas districts.

Discussion

Fluid origin

Halogens (such as Cl or Br) can be useful in constraining fluid origins because they are conservative elements, that is, they do not partition into most rock-forming minerals. Consequently, halogen ratios typically are not modified during fluid-rock interaction and are representative of the ratios acquired at the source. Conversely, the absolute concentrations and ratios of many other major and minor elements can be significantly altered as the fluid reacts with the rocks it resides within or passes through. Indeed, these changes are important indications of the reactions that may have taken place in both the basin source region and in the aquifer.

The Br-Cl systematics of those inclusions yielding bromide values in the present study suggest that the brines analyzed are generally Br enriched compared to seawater and derived their salinity from the evaporation of seawater beyond the point of halite precipitation (Fig. 8). This is consistent with the findings of Viets et al. (1996) who concluded, based on bulk analyses of inclusion fluids in sphalerite, that the ore fluids in the Northern Arkansas and Tri-State districts were composed predominantly of evaporatively concentrated seawater, with a smaller but significant component of salinity derived from halite dissolution. In the present study, the absolute concentrations of chloride, which Viets et al. (1996) were not able to determine, are slightly lower than concentrations expected in seawater that has evaporated past the point of halite saturation. This may indicate that the fluids have subsequently been diluted by meteoric water, although compositional differences can also be accounted for by differences between the chemistry of the paleoseawater that was being evaporated and modern seawater (e.g., Lowenstein et al., 2003).

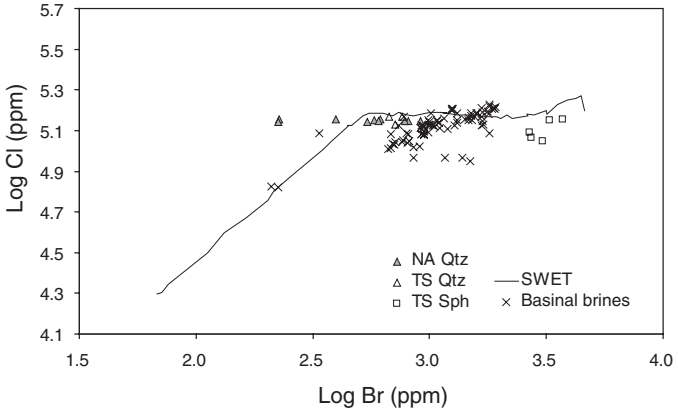

FIG. 8. Halogen systematics of measured inclusion fluid compositions from the Tri-State and Northern Arkansas districts. Limited sphalerite data suggest entrapment of significantly more Br-rich brines in this mineral. Seawater evaporation trajectory based on the data of McCaffrey et al. (1987). Basinal data from Carpenter et al. (1974).

Four analyses of the unusually low Br (type 1_{NA}) fluid inclusions hosted in quartz from the Northern Arkansas district lie away from the seawater evaporation trajectory. Of these analyses, three come from sample NAMC-1 Chip 6. Inclusion 5 from this chip (161 ppm Br) is a large inclusion located within a few tens of micrometers of a fracture containing secondary inclusions, and it is possible that this inclusion is of secondary origin itself. Another anomalously low Br analysis comes from NAMC-1 Chip 2B inclusion 2 (146 ppm Br), which is also a large inclusion proximal to a fracture and inclusion trail of possible secondary origin. However, the chemistry of these inclusions is not anomalous in any other respect and these data are therefore considered to be possibly significant. Furthermore, there is no petrographic or chemical evidence that the other two low Br inclusions observed are not primary in origin.

It is clear that the differences in Br content between the fluids trapped in sphalerite (only obtained for samples of the type 1_{TS} and the fluids of transitional salinity from the Tri-State district) and quartz (from both the type 1_{TS} and type 1_{NA} fluids) are real, with the bulk of the analyses in quartz falling toward the lower end of the range typical of basinal fluids and the sphalerite-hosted fluids having distinctly higher Br concentrations. The role of more highly evaporated, Br-enriched brines in MVT ore formation has been noted previously for other ore districts in the United States and around the world (Viets et al., 1996; Leach et al., 2005). Unfortunately, because of the limited analyses containing detectable Br and the lack of Zn concentration data for fluid inclusions in sphalerite, it is not possible to assess quantitatively whether or not a direct correlation exists between Br concentration and dissolved metal. Nonetheless, as noted above, the fluid that precipitated sphalerite could have been transporting at least two orders of magnitude more Zn than the gangue-forming fluids, which could account for this association.

Na-Br and Cl-Br relationships also support a predominantly evaporated seawater origin for the brines (Fig. 9). However, it should be noted that these relationships are less diagnostic of seawater evaporation versus halite dissolution as a source of salinity because even small admixtures of evaporatively concentrated seawater with a dilute fluid that had dissolved some halite will produce low Na/Br and Cl/Br values indicative of seawater evaporation (Chi and Savard, 1997). Nonetheless, some useful information can be obtained by examining these relationships. Again, the most Br rich analyses in Tri-State sphalerite lie at the extreme of previous measurements. Although previous work has attributed this to the relatively large errors ascribed to characterization of Br in inclusion fluids, it is important to remember that previous analyses (such as those of Viets et al., 1996) utilized bulk methods that inevitably analyze multiple fluid inclusion generations in a single sample and tend to obscure compositional extremes. It may be that discrete pulses of very Br rich brines are commonly present, but the Br signature is diluted by other, less Br rich, fluids when analyzed in bulk. This demonstrates the advantage of LA-ICP-MS microanalysis in being able to characterize ore fluid chemistry with much greater paragenetic control and at a far higher spatial resolution than is possible by bulk techniques.

The Na-Br and Cl-Br relationships from the present study differ from earlier work in some additional ways. Viets et al. (1996) and Crocetti and Holland (1989) found that fluid inclusions in early sphalerite and octahedral galena from the Viburnum Trend had Cl/Br and Na/Br ratios lower than those of seawater, lying along the seawater evaporation trend, whereas fluid inclusions in late sphalerite and cubic galena

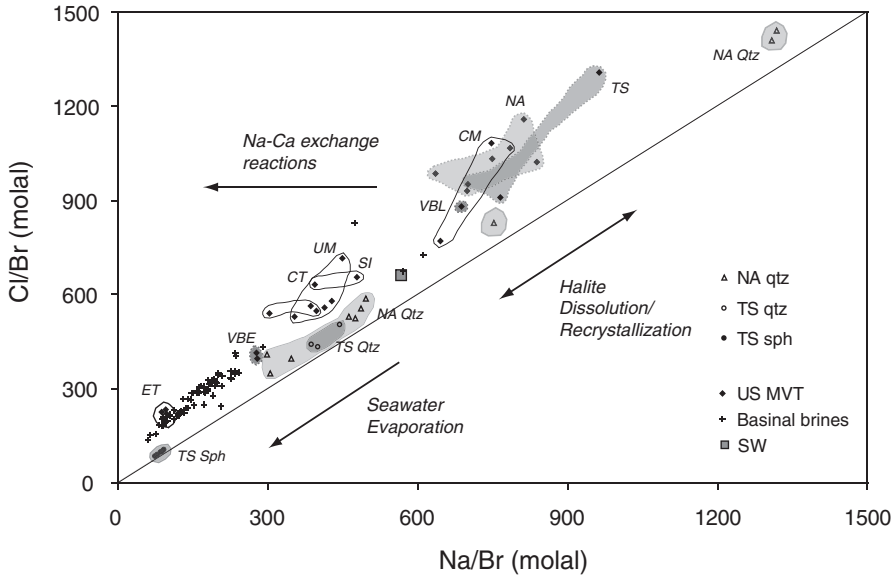

FIG. 9. Na-Cl-Br systematics of measured inclusion fluid compositions from the Tri-State and Northern Arkansas districts (shaded fields with dashed lines) compared to Tri-State and northern Arkansas data published by Viets et al. (1996, fields with solid lines). Data from additional U.S. MVT deposits published by Viets et al. (1996) are shown in unshaded fields with solid lines. CM = central Missouri, CT = central Tennessee, ET = east Tennessee, NA = northern Arkansas, SI = southern Illinois, TS = Tri-State, UM = Upper Mississippi Valley, VBE = Viburnum (early), VBL = Viburnum (late), SW = seawater. Basinal brine data from Carpenter et al. (1974).

from the Viburnum Trend and fluid inclusions from all of the other Ozark MVT deposits (Tri-State, Northern Arkansas, and Central Missouri districts) had Cl/Br and Na/Br ratios greater than those of seawater, showing a clear component of salinity derived from halite dissolution. Viets et al. (1996) considered this later fluid to indicate the effects of flushing by meteoric recharge during the later stages of the Ouachita orogeny. In contrast, in the present study, most of the fluid inclusions in samples from the Tri-State and Northern Arkansas districts had Cl/Br and Na/Br ratios lower than those of seawater, with only some of the quartz-hosted fluid inclusions from the Northern Arkansas district having values higher than those of seawater. This indicates that fluids like those that deposited early MVT mineralization in the Viburnum Trend (e.g., Crocetti and Holland, 1989) may have been more widespread in the Ozarks than previously recognized.

Major and minor elements

Based primarily on the Cl versus Br data (Fig. 8), it appears that the fluids analyzed in this study were derived predominantly from evaporated seawater. Thus, any deviations from the seawater evaporation trajectory in terms of major or minor elements can be attributed to processes occurring during diagenesis, along the ore fluid flow path, and/or at the site of mineral precipitation.

Ca concentrations of all analyses of samples from the Tri-State district are enriched relative to evaporated seawater (Fig. 10). It should be noted at this point that the seawater evaporation trajectory shown in Figure 10 is derived from modern-day analyses. A considerable body of evidence now exists from analyses of fluid inclusions in marine halites for significant differences in ocean chemistry in the Devonian-Early Permian (Lowenstein et al., 2001, 2003, 2004), the likely age range of the brines analyzed in this study. However, even with Ca levels in seawater (i.e., prior to any evaporative concentration) at twice their current level, the upper value of the range proposed by previous workers (Horita et al., 2002; Lowenstein et al., 2003), the fluids in this study are still considerably enriched in Ca relative to this putative source. This is typical of MVT fluids, has also been observed for Illinois basin brines (Lowenstein et al., 2003), and is normally attributed to either Na-Ca exchange reactions occurring during burial, such as albitization of feldspars, or to dolomitization of limestone and/or direct precipitation of dolomite, either within the basin or in the aquifer (Viets et al., 1996; Lowenstein et al., 2003; Leach et al., 2005).

Based on the Cl-Br-Na systematics (Fig. 9), albitization is considered unlikely, as there is no clear evidence of Na loss. In the case of dolomitization, Ca enrichment would be expected to be accompanied by depletion in Mg. In the Tri-State brines, Mg is present at similar levels (~1,000–1,300 ppm) in both the quartz- and sphalerite-hosted inclusions of both types 1_{TS} and 2_{TS}, and plots well below the seawater evaporation trajectory, implying that Mg has indeed been

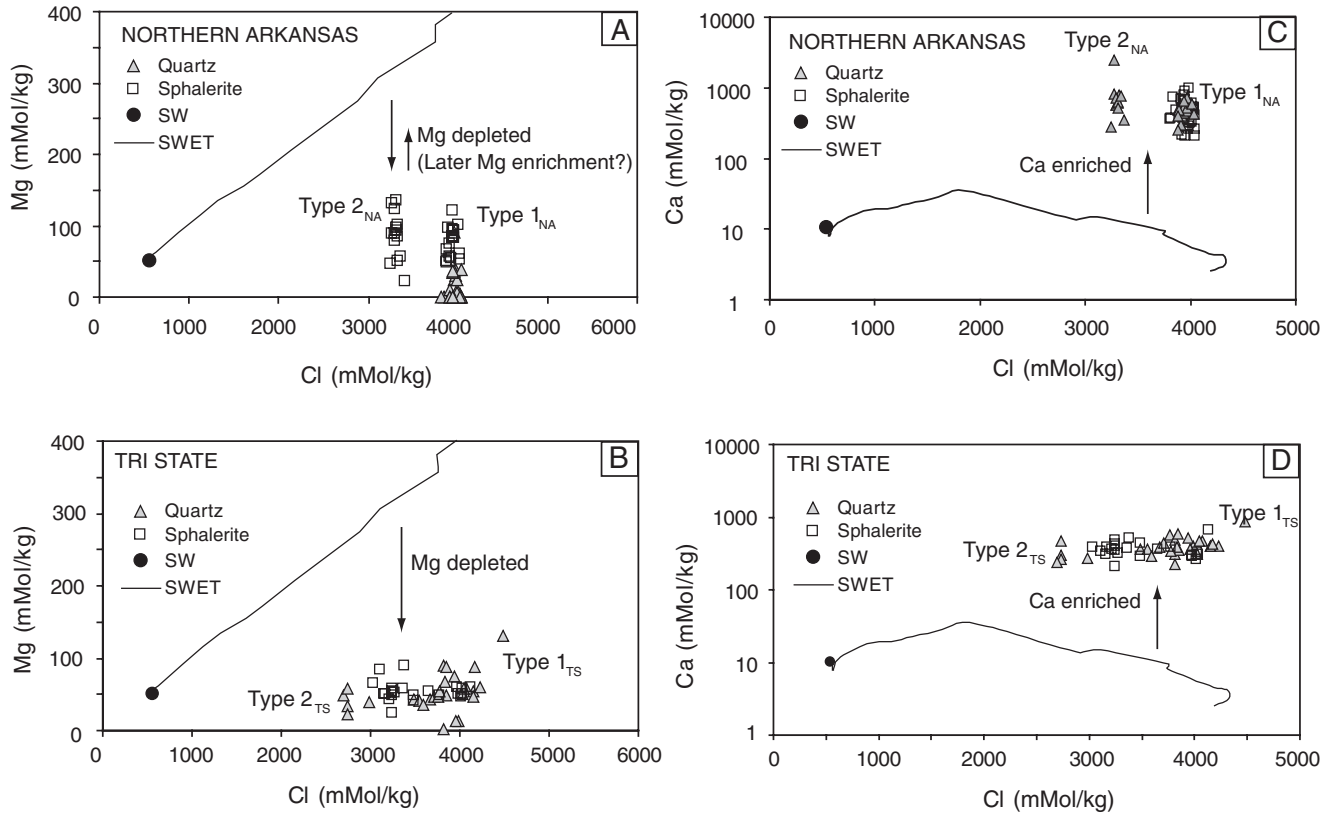

FIG. 10. Mg and Ca vs. Cl plots demonstrating that the inclusion fluids analyzed from both districts have undergone net Ca enrichment and Mg depletion relative to evaporatively concentrated seawater. It is suggested that fluids from the Northern Arkansas district underwent subsequent enrichment in Mg and Ca at the depositional site. Seawater and the seawater evaporation trajectory from McCaffrey et al. (1987).

depleted in these fluids relative to an evaporated seawater precursor (Fig. 10). The spread in data could indicate either trapping of a range of variably evaporated brines that had all become enriched in Ca and depleted in Mg to about the same degree (which seems unlikely), or that there were two differently evaporated brines that both evolved separately, losing Mg and gaining Ca, which then mixed to produce the observed spread in salinity. Results for Illinois basin brines show very similar Cl-Mg characteristics, also interpreted as due to loss of Mg from evaporatively concentrated (pre-Carboniferous) seawater via dolomitization (Lowenstein et al., 2003).

The majority of the K data for the brines preserved in fluid inclusions in samples from the Tri-State district sit relatively close to the seawater evaporation trajectory (Fig. 11) and, as observed with Ca and Mg, show a spread in salinity but not much variation in K concentration. The small deviations from evaporated seawater composition may be explained by minor dissolution and precipitation of K-bearing phases. Local processes acting to raise or lower the K concentration of the fluid significantly at the trapping site appear not to have been important.

In the Northern Arkansas district, all fluids show a Ca enrichment similar to that observed in the Tri-State district, although with a much greater variation in concentration (Fig. 10). Mg concentrations of sphalerite-hosted fluids plot below the seawater evaporation trajectory, but at a mean concentration of ~2,000 ppm are not as strongly depleted as the Tri-State fluids (Tables 5, 6). However, even relative to the Tri-State brines, the type 1_{NA} fluid preserved in quartz from the Northern Arkansas district appears to be markedly depleted in Mg, with a mean concentration of ~300 ppm. It is possible that the depletion in Mg in these type 1_{NA} fluids may relate to dolomitization of limestone, although there is no negative correlation between Mg and Ca which might be expected if this were the case (Fig. 12). However, this hypothesis is broadly consistent with the paragenesis (Fig. 2) in which the quartz trapping the type 1_{NA} fluids is late, occurring after both mineralization and precipitation of the pink dolomite.

The two sampling locations in northern Arkansas (Rush and Tomahawk Creek subdistricts) show two separate brines of different salinity that, in Ca versus Cl and Mg versus Cl space, both spread away from the seawater evaporation trajectory. This is unlike the Tri-State samples, in which the Ca and Mg versus Cl data form trends that more closely parallel the seawater evaporation trajectory (Fig. 10). This spread in the northern Arkansas data is not considered to reflect processes occurring in the source region (unless the trapping of the fluid inclusions occurred over a very extended time period), therefore the spread is interpreted to have been produced at or near the trap site, either by precipitation or dissolution of Ca- and Mg-bearing phases, such as dolomite.

If the Ca and Mg concentrations of the more uniformly Ca- and Mg-exchanged brines from the Tri-State district are taken as a possible analog for the fluid composition emerging from the aquifer in the Northern Arkansas district (i.e., prior to any modification by processes occurring at the trap site), then the type 1_{NA} and type 2_{NA} fluids recorded in sphalerite from northern Arkansas in fact would be enriched in both Ca and Mg, possibly due to dissolution of carbonate at the site of sulfide mineralization. Such dissolution could be driven by the generation of acid associated with the precipitation of sulfides. However, there is no obvious correlation between decreasing metal contents of the brine trapped in sphalerite from the Northern Arkansas district and increasing Mg concentration.

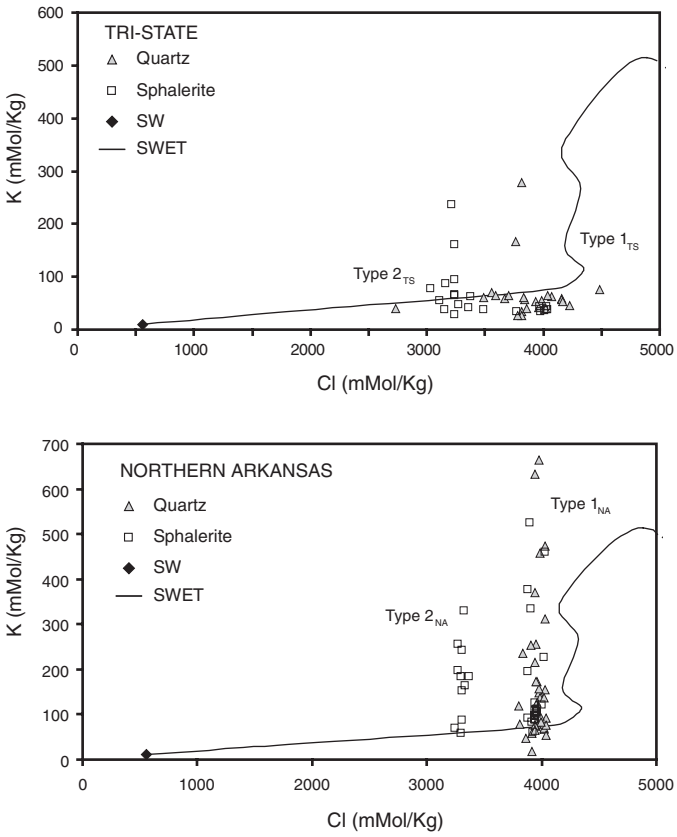

FIG. 11. K vs. Cl plots for fluids in both districts relative to evaporatively concentrated seawater. Results for Tri-State plot close to the seawater evaporation trajectory (SWET), whereas those from northern Arkansas show significant spread away from the SWET interpreted as due to variable dissolution of K-bearing phases at the depositional site. Seawater and the seawater evaporation trajectory from McCaffrey et al. (1987).

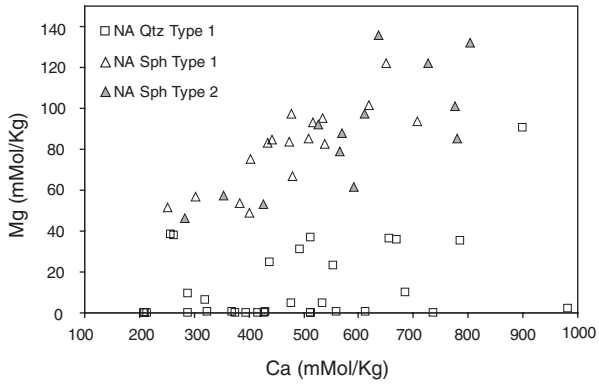

FIG. 12. Correlation between Ca and Mg in fluid inclusions in quartz and sphalerite from the Northern Arkansas district. Note that a positive correlation exists in sphalerite-hosted fluid inclusions (corresponding to carbonate dissolution) and no convincing correlation exists in quartz-hosted fluid inclusions. The contrast in Ca/Mg ratio between the different host minerals is indicative of contrasting brine compositions.

This is possibly because the metal content of this brine can only be evaluated in terms of its Pb content (as Zn cannot be characterized in these inclusions) and the precipitation event may have been dominated by sphalerite (galena is comparably rare in the Northern Arkansas district). A positive correlation between Ca and Mg is observed for the brine trapped in these inclusions (Fig. 12), with an increase of around 7 mol of Ca per mol of Mg. This is consistent with dissolution of carbonate containing approximately 14 mol percent Mg, possibly a high magnesium or partially dolomitized limestone, or a mixture of limestone and dolomite. It is noteworthy that fluids in sphalerite-hosted inclusions are markedly more Mg enriched than those in quartz (Fig. 12), reflecting different primary (basinal) and/or secondary (trap site) processes.

Compared to evaporated seawater, fluid inclusions in samples from the Northern Arkansas district show consistently elevated and highly variable K concentrations (Fig. 11). Both salinity groups (corresponding to the different sampling localities) show strong enrichment, but to different degrees, consistent with the existence of two distinct brines that evolved in a similar way in both subdistricts. It seems unlikely that the large spread observed would be caused by processes occurring in the source basin or aquifer (as observed in the Tri-State district) as this would imply a long history of infiltration of two different brines in which the K concentration gradually evolved through the whole period of trapping of these fluids in the minerals sampled. Therefore, based on an interpretation similar to that for the Ca and Mg data, the observed variation is considered more likely to represent dissolution of detrital or authigenic K-feldspar, K-mica, illite, or glauconite at the site of mineralization.

There is widespread evidence for hydrothermal dissolution in northern Arkansas (Long et al., 1986). The host limestones are known to contain glauconite locally, and congruent dissolution of magnesian limestone or dolomite containing this mineral (or perhaps other clay minerals or K-mica), possibly driven by acid generated at the site of mineralization by sulfide precipitation, could conceivably contribute to the high Ca, Mg, and K concentrations of the fluid. However, no simple correlation exists between K and either Ca or Mg, perhaps because the K-bearing phase was not distributed evenly through the rock digested by the ore fluid, and some fluids dissolved more of this mineral than others.

Based on the major element chemistry presented above, the interpretation of initial fluid evolution in both districts is very similar. Both districts are interpreted to preserve evidence of at least two brines, originally evaporated to different degrees and thus acquiring different halogen concentrations, which then underwent similar evolution pathways during basin diagenesis. This is unsurprising as, at the broad scale, basinal processes would be expected to affect large areas and modify brine chemistry in similar ways. However, during expulsion, flow, and ultimately mineralization, the chemical evolution of the brine types in the two districts diverged in response to a variety of local processes, finally being trapped as fluid inclusions with contrasting chemical compositions.

Metals

The measurement of high Pb only in sphalerite-hosted fluid inclusions is an important result as it suggests the possible invasion of unusually metalliferous brines into both the Tri-State and Northern Arkansas districts at the time of mineralization. By contrast, the Pb and Zn concentrations of the fluids that deposited quartz gangue in both districts (and dolomite in the Tri-State district) are very low, even compared to typical basinal brines (Fig. 6). This is unexpected for brines of this temperature and salinity range. If extractable metal was present in the basinal source region or along the fluid flow path through the aquifer, the metal contents of these brines could have been as much as two orders of magnitude higher (Carpenter et al., 1974; Hanor, 1996). One possible explanation for the low metal concentrations in the inclusions, assuming that the pH and redox state of the brines was within the range typical of basinal fluids, is a greater concentration of H_2S in the fluids which would have inhibited the transport of significant Pb or Zn in solution. However, the generally low Ba and Mn concentrations in all fluid types might imply relatively oxidizing conditions for both metalliferous and barren fluids alike, which would tend to favor metal transport even with elevated total sulfur (e.g. Cooke et al., 2000). Alternatively, these metal-poor brines may represent "spent" fluids that already precipitated sulfides. In northern Arkansas this is consistent with the timing of coarse quartz precipitation, which is believed to have postdated the main stage of sulfide mineralization (Fig. 2), but in the Tri-State district this does not explain results from pink dolomite which is inferred immediately to predate and overlap with mineralization (Fig. 2).

The LA-ICP-MS analyses clearly reveal that the type 1 brines responsible for quartz and sphalerite precipitation in both the Northern Arkansas and Tri-State districts were chemically distinct, despite having very similar microthermometric properties. Therefore, the division of the fluid types can be further subdivided into type $1_{NA\text{-}Q}$ and type $1_{NA\text{-}S}$ and type $1_{TS\text{-}Q}$ and type $1_{TS\text{-}S}$ to denote fluids of type 1 trapped in quartz and sphalerite, respectively (Table 7).

Deposit genesis

The identification of two geochemically distinct fluid types, one essentially barren of ore metal and responsible for the deposition of quartz (and dolomite) gangue and the other a metal-enriched, Br-rich fluid trapped in sphalerite, suggests that deposit formation in both the Tri-State and Northern Arkansas districts can be linked to incursion of a more highly evaporated fluid carrying greater concentrations of ore metals. This argues against genetic models that appeal to the cooling of a single fluid (as this requires both metals and reduced sulfur to be transported in the same fluid), such as that favored by Plumlee et al. (1994). From the data collected in this study, there is permissible evidence of fluid mixing in the genesis of the deposits in the Tri-State district. In the Northern Arkansas district, the fluid inclusion data do not provide clear evidence of district-scale mixing, although it should be noted that the present data set is derived from a relatively small number of sample locations and may not have captured evidence for this process if it occurred. Mineralization in the Northern Arkansas district appears to have coincided with strong carbonate dissolution. This carbonate dissolution could have triggered sulfide deposition through an increase in pH (Lichtner and Bino, 1992). Alternatively, if sufficient organic

TABLE 7. Summary of Fluid Inclusion Types in Quartz and Sphalerite from the Tri-State and Northern Arkansas Districts Identified by Microthermometry and Refined by LA-ICP-MS Microanalysis

District	Micro-thermometry	LA-ICP-MS	Comment
Tri-State	Type 1_{TS}	Type $1_{TS\text{-}Q}$	Metal-poor (~1 ppm Pb, 6 ppm Zn) Low Br (715 ppm)
		Type $1_{TS\text{-}S}$	Metal-poor (~1 ppm Pb) High Br (3500 ppm)
	Type 2_{TS}	Type 2_{TS}	No detectable metal No detectable Br
	Transitional	Transitional	Up to 95 ppm Pb, high Br (2,800 ppm); broadly similar to type $1_{TS\text{-}S}$ but lower salinity
N. Arkansas	Type 1_{NA}	Type $1_{NA\text{-}Q}$	Metal-poor (<1 ppm Pb, ~3 ppm Zn) Low Br (500 ppm)
		Type $1_{NA\text{-}S}$	Metal-rich (up to 400 ppm Pb)
	Type 2_{NA}	Type 2_{NA}	Metal-rich (up to 370 ppm Pb)

material was present in the host rock, its dissolution could have caused reduction of sulfate in solution thereby driving sulfide deposition.

Importantly, the barren and metalliferous brines documented in this study appear to have evolved separately from the point at which they acquired their halogen (and to some extent other elements) systematics by evaporation of seawater at the surface, through burial, diagenesis, expulsion, and transport to the ore environment. The fact that mineralization is linked to the more highly evaporated brines strongly suggests that these are more effective at scavenging and transporting Pb and Zn, and/or that they evolved within stratigraphic intervals with greater metal availability. Given that the microthermometric data show that these sphalerite-hosted ore fluids do not differ significantly from the fluids depositing quartz with regard to salinity or temperature, any difference in their metal-carrying capacity must either relate to differences in pH, redox state, or total sulfur content, and/or derivation from a distinct sedimentary package. In any case, having probably flowed through the same aquifer units as the nonmineralizing fluids en route to sites of mineralization, it seems likely that whatever process or processes made these brines potential ore fluids can be traced back to the host basin and relates to the sedimentary package with which the respective fluids equilibrated during burial and diagenesis. This is a significant conclusion, as it suggests that the genesis of these deposits is linked to the generation of brines within specific sedimentary packages in the Arkoma basin sedimentary sequence.

Modeling fluid evolution

Further implications of the data acquired from the present study were explored through geochemical solubility and speciation calculations carried out using the Geochemist's Workbench® software (Bethke, 2004). In these calculations, the concentrations of Na, Mg, Cl, K, Ca, and Pb were constrained by the fluid inclusion LA-ICP-MS data, and concentrations of HCO_3^-, Al, SiO_2, H_2S, and Zn were controlled by saturation with respect to dolomite, muscovite, quartz, galena, and sphalerite, respectively. In addition to the concentrations of chloride, metals, and sulfur, pH and the redox state of the fluid are important. Some of these relationships are evaluated in Figure 13a, which shows the concentration of sulfide in equilibrium with galena as a function of pH and aqueous Pb concentration in a ~4 *m* Cl solution with concentrations of the other major elements fixed at approximately the average of those in sphalerite-hosted fluid inclusions from the two districts shown in Tables 5 and 6. The fluid was modeled at 100ºC and had a log f_{O_2} value of –60, based on previous studies of

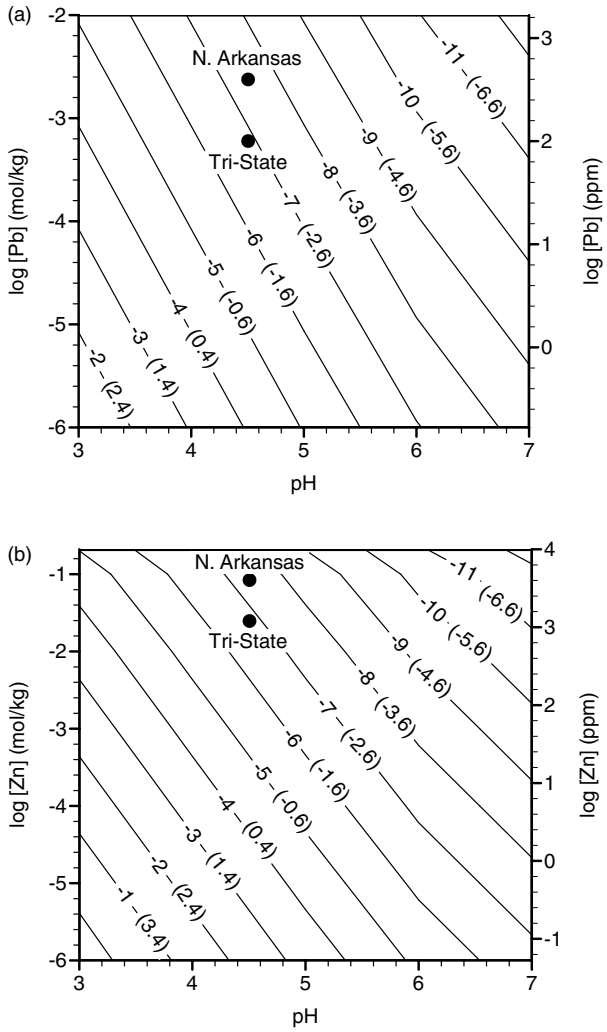

FIG. 13. (a). Contour plot of log molal sulfide concentrations in equilibrium with galena as a function of pH and Pb concentration in a 4-*m* chloride solution at 100°C and log f_{O_2} = –60. Other major element concentrations are approximately equal to the average of the Tri-State and Northern Arkansas districts means for sphalerite-hosted fluid inclusions. The contour values shown in parentheses represent log ppm sulfide concentrations. (b). Contour plot of aqueous sulfide concentrations as for (a) but for equilibrium with respect to sphalerite instead of galena. In both plots, the dark circles in the interior of the plots represent possible sulfide concentrations in equilibrium with galena at a Pb concentration of 100 ppm for the Tri-State and 400 ppm for the Northern Arkansas districts at a pH of 4.5.

basinal fluids (e.g., Anderson, 1973; Sverjensky, 1984, 1986; Plumlee et al., 1994; Hanor, 1996; Cooke et al., 2000). Figure 13b shows results of an analogous calculation but where the fluid is in equilibrium with sphalerite instead of galena.

In the Tri-State district, the high Pb concentration data are somewhat uncertain in absolute magnitude but may approach 100 ppm. In the Northern Arkansas district, high aqueous Pb concentrations can be established with greater certainty and reach approximately 400 ppm. Based on the assumptions above and a moderately acidic pH of 4.5 (Hanor, 1996), the Tri-State fluid could have carried no more than ~4×10^{-3} ppm (or 2×10^{-7} *m*) sulfur. Assuming equilibrium with sphalerite, the modeling suggests that these fluids could have contained ~1,300 ppm Zn. By contrast, the sphalerite-forming fluid in the Northern Arkansas district could have carried a maximum of only 1×10^{-3} ppm (or 4×10^{-8} *m*) sulfur but ~4,000 ppm Zn.

If the fluid that transported the elevated concentrations of Pb was also responsible for delivering sulfide to the sites of mineralization, then relatively long periods of time or very high fluid flow rates would have been required to account for the observed amounts of ore. If the pH of the mineralizing fluid was between 4 and 5, a range commonly cited as likely for MVT fluids (Anderson, 1973; Sverjensky, 1984; Plumlee et al., 1994), then a fluid carrying 100 ppm Pb could only have transported about 3×10^{-2} to 3×10^{-4} ppm sulfide (1×10^{-8} to 1×10^{-6} *m*). Figure 14 shows the results of a mass-balance calculation in which the number of years needed to deposit all of the sphalerite in the Oronogo-Duenweg trend of the Tri-State district is shown as a function of Darcy fluid flux and log of the molal sulfur concentration. The Oronogo-Duenweg orebody was chosen for the mass-balance calculation because it is a major orebody with a linear northwest-southeast orientation that is closely aligned with the presumed northerly direction of flow of the mineralizing fluids (Appold and Nunn, 2005), allowing a cross-sectional area for flow to be more easily defined. The width of the cross-sectional area was estimated to be about 1,500 m, equal to the average width of the orebody, and the height of the cross-sectional area was assumed to be 122 m, the maximum thickness of the Boone Formation in the district (Brockie et al., 1968).

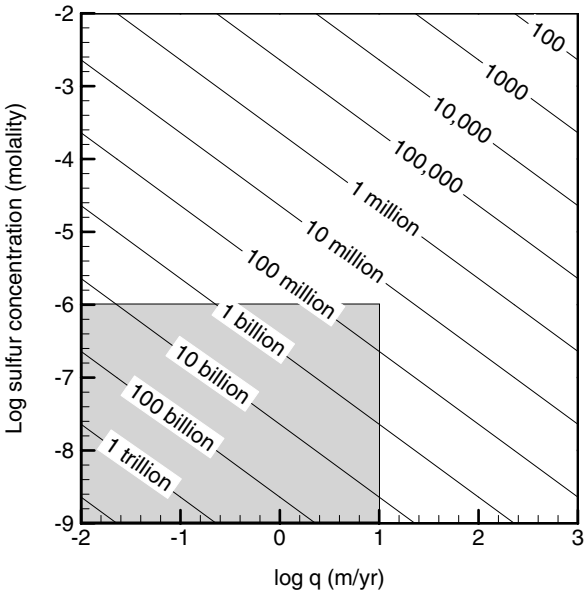

FIG. 14. Contour plot showing the log of the number of years needed to deposit 70 M tons of 4.5 percent zinc ore in the Oronogo-Duenweg trend in the Tri-State district as a function of the Darcy flux and sulfur concentration of the mineralizing fluid. Calculations assumed a cross-sectional area for flow of 1,500 × 122 m. The shaded box in the lower left corner of the plot represents the region defined by a fluid carrying at least 100 ppm Pb, which requires that the molal sulfide concentration be less than about 10^{-6} *m*, and fluid flowing with a Darcy velocity of no more than 10 m/yr. Only at the highest range of likely flow rates would the fluid be able to deposit all of the ore within a geologically reasonable period of time. Note that the shaded box could extend indefinitely lower and farther to the left than shown, because sulfur concentrations and Darcy velocities could conceivably be lower than the minimum values included in the plot.

Even for a maximum sulfide concentration of 10^{-6} *m*, corresponding to a low pH of about 4 at a Pb concentration of about 100 ppm, Darcy fluxes on the order of 10s of meters per year would have been required to deposit all of the Oronogo-Duenweg ore in less than 10 m.y. (Fig. 14). Considering that a high regional hydraulic gradient would be on the order of 10^{-2} m of hydraulic head per meter of distance then, by Darcy's law, the hydraulic conductivity would had to have been on the order of at least 10^3 m/yr, a value that is higher than the maximum reported for nonkarst carbonate aquifers but is within the range of values for karst aquifers, which may extend to 10^5 m/yr (Freeze and Cherry, 1979). Much of the mineralization, at least in the Tri-State district, occurs in breccias thought to have a karstic origin. However, karst terrane is not known to extend continuously in the Boone Formation along the presumed flow path through the Ozark platform. Thus a high degree of fluid focusing through the mineralized karst zones from the less permeable surrounding region would be required to maintain the locally high fluid fluxes.

Based on mass-balance considerations, therefore, the possibility of simultaneous metal and sulfide transport cannot be ruled out, due largely to uncertainties in the pH of the mineralizing fluid, the time available for mineralization, and the hydraulic conductivity of the host rock. However, the calculations show that this is unlikely.

The fluid inclusion LA-ICP-MS data, particularly from the gangue stages of mineralization, also indicate the presence of metal-poor brines with Pb concentrations on the order of 10^{-1} ppm or less. Reducing the Pb concentration values in the solubility and speciation calculations to 0.1 ppm, while retaining the same values for the other parameters shows that zinc concentrations would still remain higher than Pb at about 1 ppm, but the fluid could (assuming sphalerite and galena saturation) have contained up to 4 ppm total sulfide. In this case, the sulfide concentrations in these fluids would have been high enough that mixing with the more metal-rich fluids could have been an effective mechanism for sulfide precipitation. Given the evidence presented in previous sections for fluid mixing in the Tri-State district, it seems that this is the most likely mechanism by which the ore was deposited.

A further mass-balance consideration is the amount of fluid that would be needed, particularly for the giant Tri-State district. The original tonnage of ore for the whole district is estimated to have been about 500 M short tons averaging 2.2 percent Zn and 0.6 percent Pb (Brockie et al., 1968). In order to

deposit all of the Tri-State Pb from a fluid with a Pb concentration of 100 ppm, about 2×10^{10} m^3 of fluid would be needed. If the fluid travelled through an aquifer with a thickness of 100 m and a porosity of 15 percent for a distance of 200 km from the Arkoma basin to the Tri-State district, then the aquifer need only have been 7 km wide to accommodate the volume of pore fluid needed to deposit all of the Tri-State Pb. If this same fluid was saturated with respect to sphalerite so that it contained 4,000 ppm Zn, then all of the Tri-State Zn could have been deposited from an even smaller volume of fluid, about 2×10^9 m^3. Thus, even if only one pore volume of fluid along the flow path was available for mineralization, as is likely if the mineralizing fluid was evaporatively concentrated seawater expelled from a single stratigraphic interval, then the volume of fluid needed to deposit the Tri-State ores could reasonably have been derived from the volume of rock available.

Conclusions

From the data collected in this study, it appears likely that MVT mineralization in both the Tri-State and Northern Arkansas districts of the Ozark plateau was produced by incursions of metalliferous brines of distinct geochemistry carrying up to several hundred ppm Pb and up to 4,000 ppm Zn, the latter estimated from solubility constraints. These brines were Br rich and appear to have derived their salinity from evaporation of seawater past the point of halite precipitation. In contrast to these ore fluids, metal-poor brines with similar temperature-salinity characteristics were associated with deposition of gangue phases during barren stages.

The analysis of Br in individual fluid inclusions in quartz and sphalerite has revealed that the ore and gangue phases were deposited by different brines exploiting the same flow path. This finding represents a significant improvement in the resolution at which ore-forming processes can be examined. The fluid heterogeneity and multistage evolution of this hydrothermal system would not have been resolvable using traditional methods such as microthermometry or bulk techniques.

It seems likely that in the Tri-State district, sulfide deposition was triggered by mixing of the metal-rich brine and another fluid, possibly high in reduced sulfur, since the metal contents of this ore-forming brine were at the extreme upper limit of those that would permit transport of sufficient reduced sulfur to produce the observed mineralization in a geologically reasonable time. Alternatively, the metal-rich brine could have transported sulfate, which could have been reduced at the deposit sites to cause sulfide mineral deposition. In the Northern Arkansas district, fluid inclusion data from the relatively sparse geographic distribution of the samples analyzed so far do not show any evidence of fluid mixing at a district scale. The high metal Pb contents of sphalerite-hosted fluid inclusions probably require either reduction of sulfate in the fluid or mixing with a reduced sulfur-rich fluid. The ranges of major and minor element concentrations are best explained by significant dissolution of the carbonate host during mineralization, although whether this represents the cause or an effect of sulfide mineral precipitation is open to interpretation.

We conclude that MVT mineralization in these districts required the input of anomalously metal-rich fluids, which became metal rich by virtue of physical and chemical characteristics acquired early in their history and/or residence within favorable source rocks. These fluids were only expelled at a distinct stage of basin evolution, with much of the brine migration resulting in the precipitation of gangue assemblages only. These deposits are not, therefore, simply the product of typical basin evolution, helping explain why MVT mineralization may be abundant in some forelands but not in others.

Acknowledgments

This work was funded by an Albert Julius bursary to BS at Imperial College London, with additional support from the Society of Economic Geologists' Hugh E. McKinstry fund and the Institute of Materials, Minerals and Mining. Laboratory support and facilities were provided by the Natural History Museum-Imperial College Joint Analytical Facility. We thank Barry Coles and Liz Morris for technical assistance.

July 7, 2007; September 17, 2008

REFERENCES

Allan, M.M., Yardley, B.W.D., Forbes, L.J., Shmulovich, K.I., Banks, D.A., and Shepherd, T.J., 2005, Validation of LA-ICP-MS fluid inclusion analysis with synthetic fluid inclusions: American Mineralogist, v. 90, p. 1767–1775.

Anderson, G.M., 1973, The hydrothermal transport and deposition of galena and sphalerite near 100°C: Economic Geology, v. 68, p. 480–492.

——1975, Precipitation of Mississippi Valley-type ores: Economic Geology, v. 70, p. 937–942.

Appold, M.S., and Garven, G., 1999, The hydrology of ore formation in the southeast Missouri district: Numerical models of topography-driven fluid flow during the Ouachita orogeny: Economic Geology, v. 94, p. 913–936.

Appold, M.S., and Nunn, J.A., 2005, Hydrology of the western Arkoma basin and Ozark platform during the Ouachita orogeny: Implications for Mississippi Valley-type ore formation in the Tri-State Zn-Pb district: Geofluids, v. 5, p. 308–325.

Appold, M.S., Numelin, T.J., Shepherd, T.J., and Chenery, S.R., 2004, Limits on the metal content of fluid inclusions in gangue minerals from the Viburnum Trend, southeast Missouri, determined by laser ablation ICP-MS: Economic Geology, v. 99, p. 185–198.

Barnes, H.L., 1979, Solubilities of ore minerals, *in* Barnes, H.L., ed., Geochemistry of hydrothermal ore deposits, 2nd ed.: New York, John Wiley and Sons, p. 404–460.

Barrett, T.J., and Anderson, G.M., 1988, The solubility of sphalerite and galena in 1–5 m NaCl solutions to 300°C: Geochimica et Cosmochimica Acta, v. 52, p. 813–820.

Bethke, C.M., 2004, The Geochemist's Workbench® Release 5: GWB Reference Manual: Urbana, Illinois, University of Illinois, 225 p.

Bodnar, R.J., 1993, Revised equation and table for determining the freezing point depression of H_2O-NaCl solutions: Geochimica et Cosmochimica Acta, v. 57, p. 683–684.

Brockie, D.C., Hare, E.H., Jr, and Dingess, P.R., 1968, The geology and ore deposits of the Tri-State district of Missouri, Kansas and Oklahoma, *in* Ridge, J.D., ed., Ore deposits of the United States, 1933–1967: The Graton-Sales Volume: New York, American Institute of Mining, Metallurgical and Petroleum Engineers, p. 400–430.

Buckroyd, C.C., 2008, Development of the 213-nm UV laser ablation ICP-MS technique for fluid inclusion microanalysis and application to contrasting magmatic-hydrothermal systems: Unpublished Ph.D. dissertation, Imperial College, University of London, 480 p.

Carpenter, A.B., Trout, M.L., and Pickett, E.E., 1974, Preliminary report on the origin and chemical evolution of lead-and-zinc–rich oil field brines in central Mississippi: Economic Geology, v. 69, p. 1191–1206.

Chi, G., and Savard, M.M., 1997, Sources of basinal and Mississippi Valley-type mineralizing brines: Mixing of evaporated seawater and halite-dissolution brine: Chemical Geology, v. 143, p. 121–125.

Collins, A.G., 1975, Geochemistry of oilfield waters: Amsterdam, Elsevier, 496 p.

Cooke, D.R., Bull, S.W., Large, R.R., and McGoldrick, P.J., 2000, The importance of oxidized brines for the formation of Australian Proterozoic stratiform sediment-hosted Pb-Zn (Sedex) deposits: Economic Geology, v. 95, p. 1–18.

Crawford, M.L., 1981, Phase equilibria in aqueous fluid inclusions, *in* Hollister, L.S., and Crawford, M.L., eds., Short course in fluid inclusions: Applications to petrology: Calgary, Mineralogical Association of Canada, p. 75–100.

Crocetti, C.A., and Holland, H.D., 1989, Sulfur-lead isotope systematics and the composition of fluid inclusions in galena from the Viburnum Trend, Missouri: Economic Geology, v. 84, p. 2196–2216.

Czamanske, G.K., Roedder, E., and Burns, F.C., 1963, Neutron activation analysis of fluid inclusions for copper, manganese, and zinc: Science, v. 140, p. 401–403.

DeLoule, E., Allegre, C., and Doe, B., 1986, Lead and sulfur isotope microstratigraphy in galena crystals from Mississippi Valley-type deposits: Economic Geology, v. 81, p. 1307–1321.

Freeze, R.A., and Cherry, J.A., 1979, Groundwater: Englewood Cliffs, New Jersey, Prentice-Hall, 604 p.

Garven, G., 1995, Continental-scale groundwater flow and geologic processes: Annual Review of Earth and Planetary Sciences, v. 23, p. 89–117.

Garven, G., Ge, S., Person, M.A., and Sverjensky, D.A., 1993, Genesis of stratabound ore deposits in the mid-continent basins of North America.1.The role of regional groundwater flow: American Journal of Science, v. 293, p. 497–568.

Günther, D., and Heinrich, C.A., 1999, Enhanced sensitivity in laser ablation-ICP mass spectrometry using helium-argon mixtures as aerosol carrier: Journal of Analytical Atomic Spectrometry, v. 14, p. 1363–1368.

Günther, D., Frischknecht, R., Heinrich C.A., Kahlert, H.J., 1997, Capabilities of an argon fluoride 193 nm excimer laser for laser ablation inductively coupled plasma mass spectrometry microanalysis of geological materials: Journal of Analytical Atomic Spectrometry, v. 12, p. 939–944.

Günther, D., Audétat, A., Frischnecht, R., and Heinrich, C.A., 1998, Quantitative analysis of major, minor and trace elements in fluid inclusions using laser ablation-inductively coupled plasma mass spectrometry: Journal of Analytical Atomic Spectrometry, v. 13, p. 263–270.

Hagni, R.D., 1976, Tri-State ore deposits: the character of their host rocks and their genesis, *in* Wolf, K.H., ed., Handbook of strata-bound and stratiform ore deposits. II. Regional studies and specific deposits: Amsterdam, Elsevier, p. 457–494.

——1986, Paragenetic sequence of the lead-zinc-copper-cobalt-nickel ores of the southeast Missouri lead district, U.S.A, *in* Craig, J.R., Hagni, R.D., Kiesel, W., Lange, I.M., Petrovskaya, N.V., Shadlum, T.N., Udubasa, G., and Augustithis, S.S., eds., Mineral paragenesis: Athens, Theophrastus Publications, p. 90–132.

Hagni, R.D., and Grawe, O.R., 1964, Mineral paragenesis in the Tri-State district of Missouri, Kansas, and Oklahoma: Economic Geology v. 59, p. 449–457.

Hanor, J.S., 1996, Controls on the solubilization of dissolved lead and zinc in basinal brines: Society of Economic Geologists Special Publication 4, p. 483–500.

Heinrich, C.A., Pettke, T., Halter, W.E., Aigner-Torres, M., Audetat, A., Günther, D., Hattendorf, B., Bleiner, D., Guillong, M., and Horn, I., 2003, Quantitative multi-element analysis of minerals, fluid and melt inclusions by laser-ablation inductively-coupled-plasma mass-spectrometry: Geochimica et Cosmochimica Acta, v. 67, p. 3473–3496.

Horita, J., Zimmerman, H., and Holland, H.D., 2002, Chemical evolution of seawater during the Phanerozoic: Implications from the record of marine evaporates: Geochimica et Cosmochimica Acta, v. 66, p. 3733–3756.

Imes, J.L., and Smith, B.J., 1990, Areal extent, stratigraphic relation, and geohydrologic properties of regional geohydrologic units in southern Missouri: U.S. Geological Survey Hydrologic Investigations Atlas HA-711–I.

Jeffries, T.E., Jackson, S.E., and Longerich, H.P., 1998, Frequency quintupled (213 nm) laser ablation microprobe inductively coupled plasma mass spectrometry: Journal of Analytical Atomic Spectroscopy, v. 13, p. 935–940.

Kharaka, Y.K., Maest, A.S., Carothers, W.W., Law, L.M., Lamothe, P.J., and Fries, T.L., 1987, Geochemistry of metal-rich brines from central Mississippi salt dome basin, U.S.A.: Applied Geochemistry, v. 2, p. 543–561.

Land, L.S., 1995, Na-Ca-Cl saline formation waters, Frio Formation (Oligocene), south Texas, USA: Products of diagenesis: Geochimica et Cosmochimica Acta, v. 59, p. 2163–2174.

Land, L.S., Macpherson, G.L., and Mack, L.E., 1988, The geochemistry of saline formation waters, Miocene, offshore Louisiana: Transactions–Gulf Coast Association of Geological Societies, v. 38, p. 503–511.

Leach, D.L., 1994, Genesis of the Ozark Mississippi Valley-type metallogenic province, Missouri, Arkansas, Kansas and Oklahoma, USA, *in* Fontboté, L., and Boni, M., eds., Sediment-hosted Zn-Pb ores: Berlin, Springer-Verlag, p. 104–138.

Leach, D.L., and Rowan, E.L., 1986, Genetic link between Ouachita foldbelt tectonism and the Mississippi Valley-type lead-zinc deposits of the Ozarks: Geology, v. 14, p. 931–935.

Leach, D.L., Sangster, D.F., Kelley, K.D., Large, R.R., Garven, G., Allen, C.R., Gutzmer, J., and Walters, S, 2005, Sediment-hosted lead-zinc deposits: A global perspective: Economic Geology 100th Anniversary Volume, p. 561–607.

Lichtner, P.C., and Bino, G.G., 1992, Genesis of Mississippi Valley-type (MVT) deposits [abs.]: Geological Society of America Abstracts with Programs, v. 27, no.7, p. 324.

Long, K.R., Kelly, W.C., Ohle, E.L., and Lohmann K.C., 1986, Ground preparation and zinc mineralization in bedded and breccia ores of the Monte Cristo mine, northern Arkansas: Economic Geology, v. 81, p. 809–830.

Lowenstein, T.K., Timofeeff, M.N., Brennan, S.T., Hardie, L.A., and Demicco, R.V., 2001, Oscillations in Phanerozoic seawater chemistry: Evidence from fluid inclusions: Science, v. 294, p. 1086–1088.

Lowenstein, T.K., Hardie, L.A., Timofeeff, M.N., and Demicco, R., 2003, Secular variation in seawater chemistry and the origin of calcium chloride basinal brines: Geology, v. 31, p. 857–860.

Lowenstein, T.K., Timofeeff, M.N., Kovalevych, V.M., and Horita, J., 2004, The major-ion composition of Permian seawater: Geochimica et Cosmochimca Acta, v. 69, p. 1701–1719.

McCaffrey, M.A., Lazar, B., and Holland, H.D., 1987, The evaporation path of seawater and the coprecipitation of Br- and K+ with Halite: Journal of Sedimentary Petrology, v. 57, p. 928–937.

McKnight, E.T., 1935, Zinc and lead deposits of northern Arkansas: U.S. Geological Survey Bulletin 853, 311 p.

McKnight, E.T., and Fischer, R.P., 1970, Geology and ore deposits of the Picher Field, Oklahoma and Kansas: U.S. Geological Survey Professional Paper 588, 165 p.

McLimans, R.K., 1977, Geological, fluid inclusion, and stable isotope studies of the Upper Mississippi Valley zinc-lead district, southwest Wisconsin: Unpublished Ph.D. dissertation, University Park, PA, Pennsylvaniana State University, 175 p.

Nunn, J.A., and Linn, G., 2002, Insulating effect of coals and organic rich shales: Implications for topography-driven fluid flow, heat transport, and genesis of ore deposits in the Arkoma basin and Ozark plateau: Basin Research, v. 14, p. 129–145.

Ohle, E.L., and Gerdemann, P.E., 1989, Recent exploration history in southeast Missouri: Society of Economic Geologists Guidebook Series, v. 5, p. 1–11.

Pan, H., Symons, D.T.A., and Sangster, D.F., 1990, Paleomagnetism of the Mississippi Valley-type ores and host rocks in the Northern Arkansas and Tri-State districts: Canadian Journal of Earth Sciences, v. 27, p. 923–931.

Pinckney, D.M., and Haffty, J., 1970, Content of zinc and copper in some fluid inclusions from the Cave-in-Rock district, southern Illinois: Economic Geology, v. 67, p. 1–18.

Plumlee, G.S., Leach, D.L., Hofstra, A.H., Landis, G.P., Rowan, E.L., and Viets, J.G., 1994, Chemical reaction path modeling of ore deposition in Mississippi Valley-type deposits of the Ozark region, U.S. midcontinent: Economic Geology, v. 89, p. 1361–1383.

Potter, R.W., II, 1971, Geochemical, geothermetric and petrographic investigation of the Rush Creek mining district, Arkansas: Unpublished M.S. thesis, Fayetteville, AR, University of Arkansas, 115 p.

Roedder, E., 1984, Fluid inclusions: Reviews in Mineralogy, v. 12, 646 p.

Seward, T.M., and Barnes, H.L., 1997, Metal transport by hydrothermal ore fluids, *in* Barnes, H.L., ed., Geochemistry of hydrothermal ore deposits 3rd ed.: New York, John Wiley and Sons, p. 435–486.

Shepherd, T.J., and Chenery, S.R., 1995, Laser ablation ICP-MS elemental analysis of individual fluid inclusions: An evaluation study: Geochimica et Cosmochimica Acta, v. 59, p. 3997–4007.

Shepherd, T.J., Rankin, A.H., and Alderton, D.H.M., 1985, A practical guide to fluid inclusion studies: London, Blackie and Son, 239 p.

Stoffell, B., 2008, Metal transport and deposition in hydrothermal fluids: Insights from laser ablation microanalysis of individual fluid inclusions:

Unpublished Ph.D. dissertation, Imperial College, University of London, 272 p.

Stoffell, B., Wilkinson, J.J., and Jeffries, T.E., 2004, Metal transport and deposition in hydrothermal veins revealed by 213 nm UV laser ablation microanalysis of single fluid inclusions: American Journal of Science, v. 304, p. 533–557.

Stueber, A.M., and Walter, L.M., 1991, Origin and chemical evolution of formation waters from Silurian-Devonian strata in the Illinois basin, USA: Geochimica et Cosmochimica Acta, v. 35, p. 309–325.

Sverjensky, D.A., 1984, Oil field brines as ore-forming solutions: ECONOMIC GEOLOGY, v. 79, p. 23–37.

——1986, Genesis of Mississippi Valley-type lead-zinc deposits: Annual Reviews in Earth and Planetary Science, v. 14, p. 177–199.

Viets, J.G., and Leach, D.L., 1990, Genetic implications of regional and temporal trends in ore fluid geochemistry of Mississippi Valley-type deposits in the Ozark region: ECONOMIC GEOLOGY, v. 85, p. 842–861.

Viets, J.G., Hostra, A.F., and Emsbo, P., 1996, Solute compositions of fluid inclusions in sphalerite from North American and European Mississippi Valley-type deposits: Ore fluids derived from evaporated seawater: Society of Economic Geologists Special Publication 4, p. 465–482.

White, D.E., 1958, Liquid of inclusions in sulfides from Tri-State (Missouri-Kansas-Oklahoma) is probably connate in origin: Geological Society of America Bulletin, v. 69, p. 1660–1661.

Wisniowiecki, M.J., van der Voo, R., McCabe, C., and Kelly, C., 1983, A Pennsylvanian paleomagnetic pole from the mineralized Late Cambrian Bonneterre Formation, southeast Missouri: Journal of Geophysical Research, v. 88, p. 6540–6548.

Wu Y., and Beales, F., 1981, A reconnaissance study by paleomagnetic methods of the age of mineralization along the Viburnum Trend, southeast Missouri: ECONOMIC GEOLOGY, v. 76, p. 1879–1894.